A Review on Photocatalysis for Air Treatment: From Catalyst Development to Reactor Design

5 authors, including:

Yash Boyjoo
Curtin University
18 PUBLICATIONS   1,234 CITATIONS

SEE PROFILE

Hongqi Sun
Edith Cowan University
185 PUBLICATIONS   6,635 CITATIONS

SEE PROFILE

Jian Liu
University of Surrey
185 PUBLICATIONS   10,882 CITATIONS

SEE PROFILE

Shaobin Wang
University of Adelaide
498 PUBLICATIONS   19,600 CITATIONS

SEE PROFILE

Some of the authors of this publication are also working on these related projects:

Design of Novel Nanostructured Electrocatalysts and Their Applications for Energy Storage and Conversion View project

Design of Nanostructured Porous Carbon as Electrode Materials for Supercapacitor Devices View project

Review

A review on photocatalysis for air treatment: From catalyst development to reactor design

Yash Boyjoo [a], Hongqi Sun [b], Jian Liu [a], Vishnu K. Pareek [a,*], Shaobin Wang [a]

[a] Department of Chemical Engineering, Curtin University, GPO Box U1987, Western Australia 6845, Australia
[b] School of Engineering, Edith Cowan University, 270 Joondalup Drive, Joondalup, Perth, WA 6027, Australia

HIGHLIGHTS

- A state of art review of photocatalysis for air purification.
- Provides an in-depth analysis of photocatalyst development.
- Discusses various aspects of photoreactor modelling.
- Presents an overview of possible intensification pathways.

ARTICLE INFO

ABSTRACT

Photocatalysis has been extensively investigated for several decades, motivated by the fascinating applications in pollution remediation, chemical synthesis, and energy innovation. However, the practical/commercial/industrial applications of photocatalysis have been restricted in the field of building materials. The low quantum efficiency in solar energy conversion and limitation of low level of pollutants in photodegradation are very difficult to solve. Air purification by photocatalytic oxidation (PCO) of various pollutants, for example volatile organic compounds (VOCs) or inorganic gaseous (NO_x, SO_x, CO, H_2S and ozone, etc) at reasonably low concentrations, appears to be more feasible for commercialization. This review firstly introduces the removal mechanism of these contaminations by PCO, and then provides detailed survey and discussion on both photocatalysts and reactor design. This paper aims to deliver fundamental and comprehensive information for paving the venue of gas-phase photodegradation to commercialized air purification.

© 2016 Elsevier B.V. All rights reserved.

Contents

---

* Corresponding author.
    E-mail address: V.Pareek@curtin.edu.au (V.K. Pareek).

Nomenclature

C_i molar concentration of species i (mol L^{-1})

$e^{a,s}$ local superficial rate of photon absorption (Einstein s^{-1} m^{-2} or moles of photons s^{-1} m^{-2})

E incident intensity at any point from all the directions (W m^{-2} or Einstein s^{-1} m^{-2} or moles of photons s^{-1} m^{-2})

g gravitational constant (m s^{-2})

h axial coordinate of an element on lamp (m)

I intensity (W m^{-2} sr^{-1} or Einstein s^{-1} m^{-2} sr^{-1} or moles of photons s^{-1} m^{-2} sr^{-1})

J_i diffusion flux of species i (kg m^{-2} s^{-1})

k apparent rate constant (m s^{-1})

K Langmuir adsorption equilibrium constant (mol m^{-2} s^{-1})

L half length of lamp (m)

$p(\Omega' \rightarrow \Omega)$ phase function for in scattering of radiation

P pressure (N m^{-2})

r radial direction (m)

r_i reaction rate of destruction for species i (kg m^{-3} s^{-1})

R lamp radius (m)

s, z distance (m)

S_M momentum sink (kg m^{-2} s^{-2})

v velocity vector (m s^{-1})

Greek letters

θ angular coordinate

κ absorption coefficient (m^{-1})

λ wavelength (nm)

ρ density (kg m^{-3})

σ scattering coefficient (m^{-1})

τ viscous stress tensor (hydrodynamics modelling, N m^{-2})

ϕ angular coordinate of an element of lamp (lamp emission model)/monolith photon absorption efficiency

η radius of lamp-element in volume source model (lamp emission model, m)/factor giving the uniformity of irradiation of the front surface a monolith

Ω solid angle (steradian)

Φ quantum yield (mol Einstein^{-1} or mol mol of photons^{-1})/photonic efficiency

φ angle between normal to point of emission and radiation direction (lamp emission model)

Subscripts

P pollutant

S catalyst surface

w water

λ wavelength dependent

Other symbols

$\langle \rangle$ denotes volumetric of wavelength averaged values

1. Introduction

The discovery of photocatalysis in 1972 on hydrogen production by water splitting attracted immediate research interests owing to the following two energy crises, 1973 oil crisis and 1979 energy crisis. In the study carried out by Fujishima and Honda [1], a semiconductor of TiO$_2$ electrode was used to facilitate hydrogen evolution under irradiations. Once semiconductor particles are employed, provided the different sites of one particle can perform as anodes and cathodes, a myriad of photoelectrochemical cells are then produced [2]. The scope of photocatalysis, based on semiconductor mechanism, was then greatly broadened, with a variety of practical implications, such as photooxidation/photodegradation [3], photocatalytic CO$_2$ reduction [4], photocatalytic synthesis [5], photocatalytic gas-phase oxidation [6], photocatalytic removal of heavy metals [7], and photoinduced self-cleaning [8].

The extensive experimental and theoretical progresses in photocatalysis had enabled a number of excellent reviews, which paved the fundamentals of photocatalysis varying from activated surface, charge production, surface reactions to applications [9–12]. In earlier studies, most photocatalytic reactions were conducted on wide-band semiconductors, such as TiO$_2$ and ZnO. The restrictions of photocatalysis were believed to be both thermodynamic and kinetic limitations as a whole. The nature of

Table 1
Concentration limits of air pollutants (mg.m^{-3}) excluding heavy metals.

Pollutants	Average time	WHO [45]	US EPA [46]	EU Environ. [47]	China MEP (residential area) [48]	Australian Environ. [49]
PM$_{10}$	Short	0.05 (24 h)	0.035 (24 h)	0.05 (24 h)	0.05 (24 h)	0.05 (24 h)
	Annual	0.02		0.04	0.04	
PM$_{2.5}$	Short	0.025 (24 h)	0.035	N/A	0.05 (24 h)	0.025 (24 h)
	Annual	0.01	0.012	0.025	0.04	0.008
NO$_2$	Short	0.2 (1 h)	0.1 (1 h)	0.2 (1 h)	0.08 (24 h)	0.12 (24 h)
	Annual	0.04	0.053	0.04	0.04	0.03
SO$_2$	Short	0.5 (10 min)	0.075 (1 h)	0.35 (1 h)	0.05 (24 h)	0.20 (24 h)
	Annual	0.02 (24-h)	0.5 (3 h)	0.125 (24 h)	0.02	0.02
CO	Short	N/A	10 (8 h)	10 (8 h)	10 (1 h)	9 (8 h)
	Annual	N/A			4 (24 h)	
O$_3$	Hourly	0.1 (8 h)	0.07 (8 h)	0.12 (8 h)	0.12 (1 h)	0.1 (1 h)
						0.8 (4 h)
VOCs	Short	N/A	N/A	Benzene: 0.005 (annual)	Benzopyrene: 0.000001 (annual)	N/A
	Annual	N/A	N/A	PAHs: 0.000001 (annual)		

a photocatalyst material determines the absorption of photons and the following charge production, recombination and migration. The initial step, light absorption, also governs the utilization efficiency of solar energy, in which ultraviolet (UV) light that can be harvested by TiO$_2$ or ZnO only represents less than 4% solar spectrum energy [13,14]. Once the photoinduced charges successfully migrate to the surface, where photocatalytic reactions take place, they could still undergo surface recombination or be trapped by undesirable reactants. As such photocatalysis efficiency has remained at a very low level.

With more than four-decade development, photodegradation of either aqueous or gaseous pollutants, and production of solar fuels by photocatalytic either water splitting or CO$_2$ conversion, have been the hottest topics in photocatalysis. In the ISI database, 5840 results come up when "photodegrad*" is set in "Topic" and "2013–2015" is set for "Year published". The results becomes 6788 when the "Topic" is changed to "photocata*" and "hydrogen or (CO$_2$ reduction)". It can be seen that research activities have followed the edges of research gap, either material adventures [15–20] or theoretical studies [21–24], yet the gap between research and practical application is still not resolved. Commercial photocatalysis has to be both technically and economically competitive to counterpart technologies, for example hydrogen production from hydrocarbon reforming [25,26], CO$_2$ conversion by dry reforming and chemical synthesis [27–29], water treatment by adsorption [30,31], biological treatment [32,33] or advanced oxidation processes (AOPs) [34–36]. Compared to above industrial processes, air purification especially indoor air purification appears to be a promising field in which photocatalysis could potentially act as a commercialized technology, integrating with particulate matter removal technologies.

The severe heath effect of air pollution has been worldwide recognized for a long time [37]. Two main categories of air pollutants, e.g. particulate matters (PM) and gaseous pollutants, have been identified to be the main concerns. Both source control and air cleaning have been demonstrated to be effective strategies for tackling the air pollutants. For indoor air pollution, increasing ventilation can be also effective [38]. For the issue of particulate matters (PM$_{2.5}$ and PM$_{10}$), source control [39,40] and physical treatments, such as electrostatic precipitation [41], wet scrubbing [42], and filtration [43], can be employed. It is unlikely that photocatalysis can deal effectively with particulate pollutants, so in this review, we will focus on the photocatalytic removal of gaseous pollutants, including NO$_x$ (mainly NO$_2$), SO$_x$ (mainly SO$_2$), ozone (O$_3$), CO, odors, and volatile organic compounds (VOCs). Table 1 lists the concentration limits of selected air pollutants from some authorities. In the table, heavy metals are not included as they are out of the treatment scope of photocatalysis. It is also seen that VOCs

and odorous compounds (H$_2$S and S-containing organics) are not clearly regulated in the standards. However, the detection of such compounds in indoor air and the associated health problem such as sick building syndrome (SBS) were well confirmed [38,44]. Traditional air cleaning technologies for removing these gaseous pollutants are limited in physical methods such as ventilation, adsorption, or filtration, yet an effective strategy for destruction of such contaminants has not been developed.

The low level contaminants and fewer competitors (effective and low cost technology) for air purification, especially indoor air purification have offered a perfect job to photocatalytic oxidation (PCO), with readily commercialization at a limited scale utilizing UV. Several excellent review papers in this field have been published, with particular attention to NO$_x$ [50], SO$_x$ [51], VOCs [38,44] and odors [52]. The PCO fundamentals [53], materials aspects [54], reaction conditions in PCO for air purification [55] and its comparisons [56] were also reviewed. However, a comprehensive review covering mechanism, photocatalyst design, reactor design and simulations has not been published. In this literature survey, we aim to bridge this gap for paving the venue to commercialized PCO air purifiers.

2. Photocatalytic oxidation (PCO) for air purification

Photocatalytic water splitting has been extensively investigated in 1970s due to the energy/oil crisis, but the photocatalysis was navigated to the degradation of organic pollutants in 1980s. Analogue to the extensive studies on degradation of aqueous pollutants [5,7,9,10,12,57–59], PCO removal of gaseous pollutants was also developed.

2.1. Photodegradation of VOCs

In early 1970s, Teichner et al. [60] firstly reported gas-phase heterogeneous photocatalysis for partial oxidation of paraffins. Stone et al. [3,61] systematically investigated the photoadsorption of oxygen and PCO of isopropanol at rutile surfaces. It was shown that water and oxygen can be chemically adsorbed onto the TiO$_2$ surface, and then produce reactive species on the surface. At first, dissociative chemisorption of water at Ti^{4+}O^{2-} pairs would produce surface OH$_S^-$ and bulk OH$_L^-$ (at vacancies O$_L$(O^{2-})). On the reactive surface of TiO$_2$, OH$^-$ would trap a positive hole to produce ·OH, while surface adsorbed oxygen, O$_{2ads}$ will form O$_{2ads}^-$ with an electron [61].

$$H_2O + O_S^{2-} \rightarrow OH_S^- + OH_S^- \tag{1}$$

$$H_2O + O_S^{2-} + O_L(O^{2-}) \rightarrow OH_S^- + OH_L^- \tag{2}$$

$$2H_2O + 4O_{S,L}^{2-} + 4Ti^{4+} \rightarrow 4OH_{S,L}^{-} + 4Ti^{3+} + O_2(g) \tag{3}$$

$$TiO_2 + h\nu \rightarrow h^+ + e^- \tag{4}$$

$$OH^- + h^+ \rightarrow \cdot OH \tag{5}$$

$$O_{2,ads} + e^- \rightarrow \cdot O_{2,ads}^- \tag{6}$$

$$\cdot OH + O_{2,ads}^- \rightarrow HO_2^- + \cdot O_{ads}^- \tag{7}$$

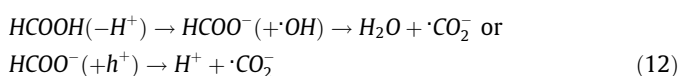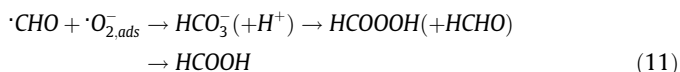$$HO_2^- + h^+ \rightarrow HO_2^{\cdot} \tag{8}$$

It is seen that surface adsorption of oxygen and water can produce reactive radicals that present in photodegradation in water [11,12,57], indicating the capability of PCO for removal of organic pollutants in air [3]. The investigations on chemisorption and photochemistry of H_2O, O_2, and CO_2 further realized the ideas of PCO removal of VOCs for air purification [9]. The increasing concern of health issue from indoor air pollution has significantly attracted worldwide attention in PCO for VOCs removal.

A wide variety of VOCs, including main contributions from aromatics, aldehydes and halocarbons, have been detected in either outdoor or indoor air. For better evaluation of the performances of photocatalysts or reactors, formaldehyde, trichloroethene (TCE), toluene and benzene have been frequently applied as typical VOCs in PCO studies.

2.1.1. PCO of formaldehyde

Formaldehyde (HCHO) as a representative carbonyl compound has been identified as the major indoor air pollutants and exposure to HCHO would lead to cancer and other serious sickness. The concentration of HCHO is usually at ppbv to ppmv levels in polluted air, while it is still much higher than the limit from WHO guideline (80 ppbv or 0.1 mg.m^{-3}) [62]. Peral and Ollis [63] firstly reported their investigations on the heterogeneous photocatalytic oxidation of a number of gaseous pollutants including formaldehyde, acetone, 1-butanol, butyraldehyde, and m-xylene. Anatase TiO_2 powders were irradiated under UV, and the degradation reactions were well described by the Langmuir-Hinshelwood rate forms. Obee et al. [64] found that humidity can significantly influence the PCO efficiency of formaldehyde, due to the competitive adsorption of water and the organic molecules. Yang et al. [65] analyzed the products and intermediates of PCO of formaldehyde, and proposed a degradation mechanism as illustrated in Eqs. (9)–(13).
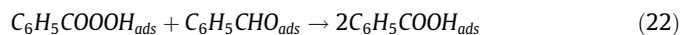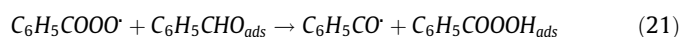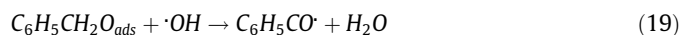
$$HCHO + \cdot OH \rightarrow \cdot CHO + H_2O \tag{9}$$

$$\cdot CHO + \cdot OH \rightarrow HCOOH \tag{10}$$

$$\cdot CHO + \cdot O_{2,ads}^- \rightarrow HCO_3^- (+H^+) \rightarrow HCOOOH (+HCHO) \\ \rightarrow HCOOH \tag{11}$$

$$HCOOH(-H^+) \rightarrow HCOO^- (+\cdot OH) \rightarrow H_2O + \cdot CO_2^- \text{ or} \\ HCOO^- (+h^+) \rightarrow H^+ + \cdot CO_2^- \tag{12}$$

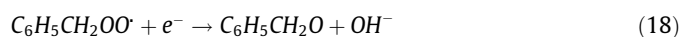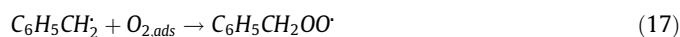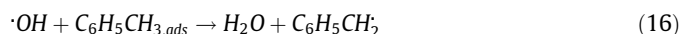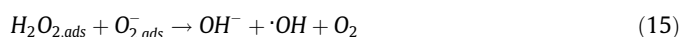$$\cdot CO_2^- (+[O] + \cdot OH + h^+) \rightarrow CO_2 \tag{13}$$

The effects of reaction conditions [66], reactors [67,68], kinetic analysis [69] and modelling [70] of PCO of formaldehyde were also investigated.

2.1.2. PCO of toluene

Toluene has been frequently detected in both indoor and outdoor polluted air so it becomes one of the most investigated model pollutants in the PCO studies. In the AFNOR standard, XP-B44-013 proposed by a French normalization group, toluene was recommended as the model pollutant for PCO evaluation [71]. Light source is very important in PCO as it controls the initial step of generation of electron-hole pairs in the photocatalysts. Jeong et al. [72] compared the efficiencies of three different UV lights, e.g. short-wavelength UV of 254 + 185 nm, 365 nm (black light blue lamp) and 254 nm (germicidal UV lamp) for PCO removal of toluene, and found that UV of 254 + 185 nm provided the highest efficiency. Quici et al. [73] carried out studies on the effect of key parameters on the PCO of toluene low concentration, which was stressed to be more realistic for the indoor air purification under UV irradiations of 254 + 185 nm. The effect of the thickness of the catalyst film was also optimized and discussed. Auguliaro et al. [74] reported their mechanistic studies on PCO of gaseous toluene. The degradation processes are described in below equations.

$$2HO_2^{\cdot} \rightarrow O_2 + H_2O_2 \tag{14}$$

$$H_2O_{2,ads} + O_{2,ads}^- \rightarrow OH^- + \cdot OH + O_2 \tag{15}$$

$$\cdot OH + C_6H_5CH_{3,ads} \rightarrow H_2O + C_6H_5CH_2^{\cdot} \tag{16}$$

$$C_6H_5CH_2^{\cdot} + O_{2,ads} \rightarrow C_6H_5CH_2OO^{\cdot} \tag{17}$$

$$C_6H_5CH_2OO^{\cdot} + e^- \rightarrow C_6H_5CH_2O + OH^- \tag{18}$$

$$C_6H_5CH_2O_{ads} + \cdot OH \rightarrow C_6H_5CO^{\cdot} + H_2O \tag{19}$$

$$C_6H_5CO^{\cdot} + O_{2,ads} \rightarrow C_6H_5COO^{\cdot} \tag{20}$$

$$C_6H_5COO^{\cdot} + C_6H_5CHO_{ads} \rightarrow C_6H_5CO^{\cdot} + C_6H_5COOOH_{ads} \tag{21}$$

$$C_6H_5COOOH_{ads} + C_6H_5CHO_{ads} \rightarrow 2C_6H_5COOH_{ads} \tag{22}$$

$$C_6H_5COOH_{ads} \rightarrow C_6H_6 + CO_2 \tag{23}$$

With the partial oxidation, benzaldehyde, benzoic acid and small concentrations of benzyl alcohol and phenol will be produced as the intermediates. Blount and Falconer [75] conducted the characterization of the species on TiO_2 after PCO of gaseous toluene, and observed a ring structure with a methyl (or oxidized methyl) groups. The produced intermediates will eventually contaminate the surface of the photocatalyst. Belver et al. [76] prepared Pd/TiO_2 photocatalysts and applied them to conduct toluene vapor PCO. They found that palladium can increase the resistance of TiO_2 to deactivation due to the less formation of benzaldehyde.

2.1.3. PCO of benzene

Benzene is another typical aromatic compound along with toluene, phenol, chlorobenzene, chlorophenols and benzoic acid. It becomes a ubiquitous contaminant derived from gasoline vapor, flue gas, chemical manufactories, paints, plastics, rubber, auto exhaust and cigarette smoke. The health issue from the exposure to even low level of benzene, such as leukemia, has been reported [77]. Wang and Ku [78] employed a batch-type photoreactor containing a bundle of TiO_2-coated quartz fibre to carry out PCO of gaseous benzene. Phenol was suggested to be the major intermediate but the final products were CO_2, CO and H_2O. Gas chromatography mass spectroscopy (GC–MS) and Flourier transform infrared spectroscopy were applied to illustrate the degradation pathways, as shown in Fig. 1 [78].

2.1.4. PCO of trichloroethene (TCE)

Trichloroethylene (TCE) is an organochloride compound that has been widely used in industry as a solvent, degreasing and/or
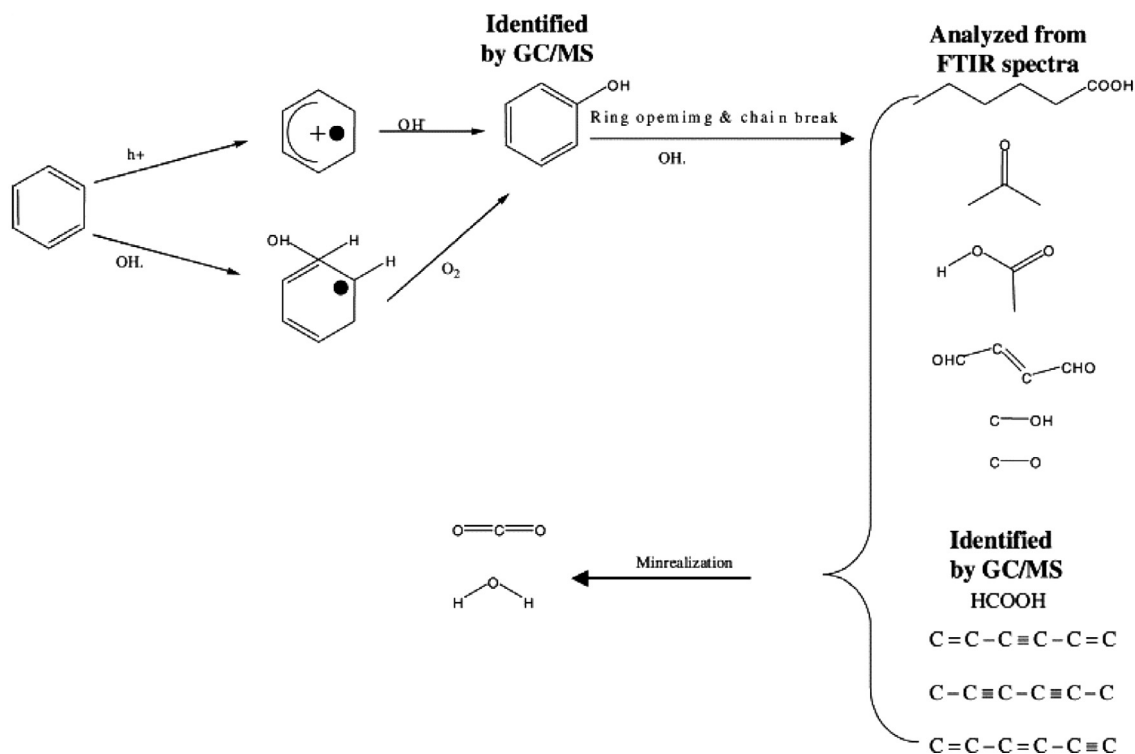
Fig. 1. Gas-phase PCO of benzene by UV/TiO$_2$ processes [78].

cleaning agent. The wide application has led to the associated contaminations to industrial emissions, landfills, hazardous waste disposal sites or indoor air. Therefore, as one of the chlorinated VOCs, TCE has been chosen as a typical air pollutant for PCO studies [79]. It was noted that the intermediates of chlorinated VOCs during PCO are more toxic and hazardous than those of other VOCs. For example, phosgene (COCl$_2$), dichloroacetyl chloride (DCAC) and trichloroacetyle chloride (TCAC), chloroform (CHCl$_3$), carbon tetrachloride (CCl$_4$), and carbon monoxide (CO) were observed in PCO process of TCE or PCE [80]. To minimize the production of toxic intermediates, Ou and Lo [81] investigated the effects of oxygen and relative humidity (RH) on the generation of DCAC and phosgene. A TCE degradation mechanism was proposed as shown in Fig. 2 [81]. It was found that the optimization of oxygen and RH can reduce the amount of the toxic intermediates.

In the PCO processes for VOCs removal, fundamental researches were almost made on TiO$_2$ photocatalysts. The development of novel photocatalysts for VOCs removal will be introduced in latter parts.

2.2. Photocatalytic removal of NO$_x$ and SO$_x$

2.2.1. Photocatalytic removal of NO$_x$

Nitric oxides can be emitted from both natural processes and human activities. For example, volcanic activity, transportation from high to low atmosphere, and some decomposition processes of organic matters due to the function of microbes in an ecosystem and solar energy can emit NO$_x$. In metropolitan areas, the NO$_x$ emissions are usually worsened by human activities, such as the combustion processes in stationary and mobile units like vehicles. Most common NO$_x$ includes NO and NO$_2$. The NO$_x$ emissions have caused both environmental and health issues, e.g. production of tropospheric ozone, acid rains, global warming and human diseases relevant to respiratory and immune systems [82]. The strategies for NO$_x$ removal include primary methods which focus on the
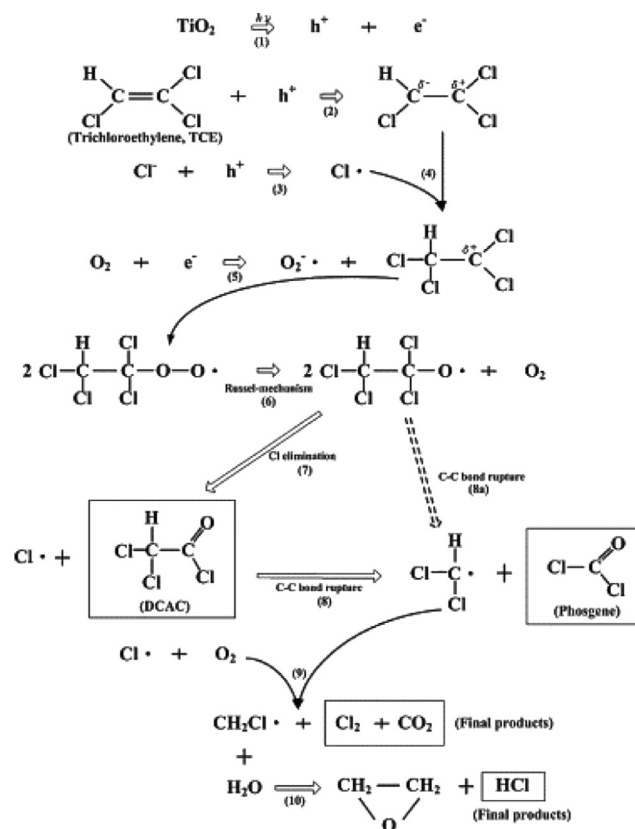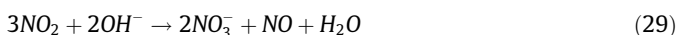

Fig. 2. Proposed mechanism of TCE photodegradation [81].

emission control, and the secondary methods to convert NO$_x$ into N$_2$ (reduction route) or HNO$_3$ (oxidation route). As a typical sec-

ondary method, heterogeneous photocatalysis can remove NO_x by three different processes, e.g. photo-decomposition, photo-oxidation, and photo-SCR (selective catalytic reduction) [50].

The photo-oxidation of NO_x is to convert NO into HNO_3 via $NO \rightarrow HNO_2 \rightarrow NO_2 \rightarrow HNO_3$ with the assistance of photocatalysis. The mechanism can be described in following equations [50].

$$NO + \cdot OH \rightarrow HNO_2 \tag{24}$$

$$HNO_2 + \cdot OH_{ads} \rightarrow NO_2 + H_2O \tag{25}$$

$$NO_2 + \cdot OH_{ads} \rightarrow HNO_3 \tag{26}$$

$$NO + \cdot O_{2,ads}^- \rightarrow NO_3^- \tag{27}$$

$$2NO + \cdot O_{2,ads}^- + 3e^- \rightarrow 2NO_2 \tag{28}$$

$$3NO_2 + 2OH^- \rightarrow 2NO_3^- + NO + H_2O \tag{29}$$

Luevano-Hipolito et al. [83–85] have carried out extensive studies on photocatalytic removal of nitric oxide. $Bi_2Mo_3O_{12}$ was demonstrated to be of excellent performance of removal of NO with 88.9% conversion in steady state by UVA PCO [85]. WO_3 polyhedral particles were prepared by a template of polyethylene glycol and showed PCO NO removal under UV irradiations [83]. The composite of TiO_2/WO_3 was also examined in the removal of NO under both UV and visible light irradiations [84].

Photo-decomposition of NO_x follows other routes that mainly apply the reduction ability of photocatalysis to form N_2 from NO_x reduction [86,87].
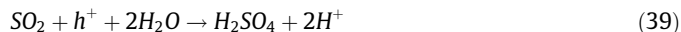
$$NO_{ads} + e^- \rightarrow N_{ads} + O_{ads} \tag{30}$$

$$NO_{ads} + N_{ads} \rightarrow N_2O_{ads} \tag{31}$$

$$NO_{ads} + O_{ads} \rightarrow NO_{2,ads} \tag{32}$$

$$2O_{ads} \rightarrow O_{2,ads} \tag{33}$$

$$2N_{ads} \rightarrow N_{2,ads} \tag{34}$$

$$2NO_{ads} \rightarrow O_{2,ads} + N_{2,ads} \tag{35}$$

$$2N_2O_{ads} \rightarrow O_{2,ads} + 2N_{2,ads} \tag{36}$$

Photo-selective catalytic reduction (photo-SCR) employs reductive reagents such as CO, hydrocarbons or NH_3 to convert NO to N_2.

2.2.2. Photocatalytic removal of SO_x

Gaseous SO_x in ambient atmosphere has been set as one of the critical pollutants by US EPA because it can lead to acid rains, vegetation damage and building corrosions. It is also one of the major precursors that can form airborne particles causing the degradation of visibility and change of climate patterns. The long-term exposure to SO_x polluted air can induce respiratory problems such as bronchi constriction and acerbated asthma [88]. Photofixation of SO_2 on anatase TiO_2 thin films was carried out by Topalian et al. [89], and they found that adsorbed SO_2 can be photo-oxidized to sulfide and sulfate surface species facilitated by the formation of reactive oxygen species.

$$SO_{2,ads} + \cdot O_{2,ads}^{2-} \rightarrow SO_{4,ads}^{2-} \tag{37}$$

$$SO_{2,ads} + \cdot OH_{ads}^- \rightarrow HSO_{3,ads}^- \tag{38}$$

Xia et al. [90] reported their studies on simultaneous photocatalytic removal of gaseous NO and SO_2 using $BiOI/Al_2O_3$ as a visible light photocatalyst. The mechanism was proposed and the conversion processes of SO_2 are shown here.

$$SO_2 + h^+ + 2H_2O \rightarrow H_2SO_4 + 2H^+ \tag{39}$$

$$SO_2 + \cdot OH_{ads} \rightarrow HSO_3 \tag{40}$$

$$SO_2 + \cdot O_{2,ads}^- \rightarrow SO_4^{2-} \tag{41}$$

The simultaneous removal of various gas pollutants can make the PCO removal of gaseous pollutants more competitive in practical applications.

2.3. Photocatalytic removal of CO and ozone

Carbon monoxide, CO, is a toxic air pollutant in safe living environments [91]. Usually it is originated from partial oxidation (combustion) of VOCs (hydrocarbons), and can be fatal due to the occupation of oxygen in blood. In general, CO oxidation to CO_2 is the last step of most degradation/oxidation reactions of VOCs. Linsebigler et al. [92] carried out a study on CO photooxidation on TiO_2 (1 1 0) and concluded that the active adsorbed molecular oxygen is important for the oxidation while lattice oxygen of TiO_2 does not involve in the reactions. The CO photooxidation with oxygen can be described by the following equations [93]. Once surface water or hydroxyl radicals are involved, carbonate groups might be formed.

$$CO + h^+ \rightarrow CO^\cdot \tag{42}$$

$$\cdot O_2^- + h^+ \rightarrow 2O \tag{43}$$

$$O + e^- \rightarrow O^- \tag{44}$$

$$O^- + CO^\cdot \rightarrow CO_2 \tag{45}$$

Ozone, a blue colored gas with a pungent odor, naturally appears in a layer between about 30,000 and 150,000 feet above the earth's surface and plays a beneficial role in the atmosphere absorbing UV for protecting the extreme UV exposure of the Earth. However, it can become a hazardous contaminant in ambient environment. It has a high oxidizing power and varies with different location, season and weather patterns. Once the concentration is higher than 0.214 mg m^{-3}, it can be toxic and hazardous to human health, causing headaches, chest pain, and irritations of eyes, nose and throat [94]. Therefore it is regulated by many organizations. With the formation of reactive radicals, photocatalysis can be used for decomposition of ozone following the equations below [95].

$$O_3 + e^- \rightarrow \cdot O_3^- \tag{46}$$

$$\cdot OH + O_3 \rightarrow \cdot O_4^- + H^+ \tag{47}$$

$$\cdot O_3^- + O_3 \rightarrow \cdot O_4^- + O_2 \tag{48}$$

More conversions were also reported [94].

$$\cdot O_4^- + O_3 \rightarrow \cdot O_3^- + 2O_2 \tag{49}$$

$$H^+ + \cdot O_3^- + \cdot O_4^- \rightarrow 3O_2 + OH^- \tag{50}$$

In fact, as a powerful oxidizing agent, ozone can be eliminated by oxidation of some VOCs in air. The simultaneous removal of various pollutants might be a new direction in this field.

2.4. Photocatalytic deodorization

Odor removal is one of the important tasks of air purification. Odor can be caused by the presence of H_2S, S-containing compounds, and some bacteria. The mechanism of PCO removal of odorous S-containing organic compounds is similar to that of VOCs [96], while the mechanism of photocatalytic deactivation of odor-

Table 2
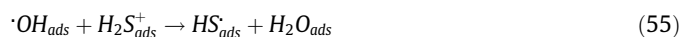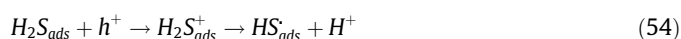Photocatalytic oxidation of VOCs on TiO₂-based photocatalysts.

Photocatalyst	Pollutant	Light source	Reactor	Reaction condition	Performance	Refs.
Silica glass fibres supported P25-Degussa TiO₂	Acetylene	UV-365 (8–10 mW/cm²)	Continuous flow quartz reactor	100 ppm acetylene in N₂ and trace water at 500 mL/min	85% mineralization rate with formaldehyde, glyoxal and formic acid as intermediates	[114]
A monolithic catalytic bed coated with P25 and PC500	Perchloroethylene (PCE) and n-decane	A solar simulator	An annular reactor	n-Decane of 71 ppm and PCE of 1095 ppm at 150 mL/min and 40% RH	100% mineralization rate for n-decane while 69% for PCE	[115]
Graphene oxide supported P25	Ethanol and benzene	UV at 25 mW/cm²	A batch reactor	Ethanol at 1.2×10^{-4} M	Around 95% conversion	[116]
TiO₂-coated flexible PVC sheet	Benzene and toluene	Natural sunlight with UV of 1.0–2.1 mW/cm²	A batch reactor of a capacity of 1920 cm³	50% RH	Rate constant of 7.65×10^{-5} and 1.07×10^{-4} min⁻¹/cm²	[117]
TiO₂-coated on optical fibre	Isopropanol	UV-LED of 126.1 mW/cm²,	A tubular optical fibre reactor	10 ppm IPA, a flow rate of 10 sccm, and 0% RH	22% IPA removal	[118]
TiO₂ thin film on window glass	Acetone and benzene	UV with 11.02 mW/cm²	A batch reactor	500 ppm acetone and 110 ppm benzene respectively	100% acetone conversion in 25 min and 100% benzene conversion in 110 min	[119]
Transparent, mechanically robust TiO₂ films	Ethanol and acetaldehyde	23 mW/cm² UV (280–400 nm) and simulated sunlight	A 7-L Pyrex glass cylindrical reactor	275 ppm (140 ppm for solar tests) in dry air of 80:20 N₂:O₂	Under UV 100% conversion in 70 min for ethanol and 125 min for acetaldehyde	[120]
Nano and micro-sized TiO₂	Acetone, acetaldehyde and toluene	UVA at 30 W/m²	A 5-L batch reactor	40% RH and mixed VOCs at 400 ppmv	PC105 (Cristal) > P25 (Evonik) > 1077 (Kronos) > AT-1 (Cristal)	[105]
TiO₂ microfibers	Acetone, heptane and toluene	UV-365 from LEDs	A batch reactor based on a PTFE gas-circulating loop	50, 100, 200 or 500 ppm acetone, 100 ppm toluene or 200 ppm heptane at 3.3 L/min, and 20% RH	Quantum efficiencies of 0.0106, 0.0027 and 0.0024 for acetone, heptane and toluene on TiO₂ fibres	[106]
Mesoporous TiO₂	Benzene	UVA of 0.19 mW/cm²	A 6.5-L batch reactor	2 μL benzene injection	About 80% conversion on TS-400 (the best prepared sample)	[107]
Anatase (F-doped) TiO₂ nanosheets with exposed 0 0 1 facets	Acetone, benzene, and toluene	UV-A of 4.97 mW/cm² and visible light (400–1000 nm) 15.04 mW/cm²	A 7.2-L batch reactor	5.2 μL acetone and 2 μL benzene injection	High efficiency under both UV and visible light	[108]
TiO₂/SiO₂ nanocomposites	Benzene	160 W high-pressure mercury lamp	A batch reactor	2 μL benzene injection	When Ti/Si = 30: 1, 92.3% conversion in 120 min, 6.8 times higher than P25	[109]
Fe₂O₃-doped TiO₂	Trichloroethylene (TCE)	UV and visible light irradiation	An annular reactor	500 ppm TCE in air at a flow rate of 250 sccm and 50% RH	95% TCE conversion	[121]
Transition metal modified TiO₂	Benzene	Vacuum ultraviolet (VUV)	A fixed-bed flow reactor	1 L/min of 50 ppm benzene and 50% RH	Mn/TiO₂ gave the highest conversion of 58%	[110]
Cu-doped TiO₂	TCE	UV365 at 1.0 mW/cm²	A continuous annular reactor	500 ppm TCE at a flow rate of 200 mL/min	0.2 wt% Cu content favoured the mobility of both TCE and water while 0.5 wt% Cu strongly blocked the active sites	[122]
V-doped TiO₂/porous polyurethane	Toluene	400–700 nm visible light	A continuous reactor	200 ppm toluene at 200 mL/min and 50% RH	80% toluene removal	[113]
Sn²⁺-doped TiO₂	Benzene	Visible light >420 nm	A fixed-bed reactor	200 ppm benzene at a flow rate of 20 mL/min	TS-40 (Ti/Sn = 40: 1) provided 27% benzene conversion	[123]
Pt/TiO₂	Cyclohexane	UV-365 from LEDs (90 mW/cm²)	A fluidized bed photoreactor	200 ppm cyclohexane, 10 vol% O₂ and 320 ppm water at 500 mL/min	100% conversion and platinum promoted the CO₂ selectivity	[111]
N-doped and O-deficient TiO₂	Benzene	Visible light (>400 nm)	Fixed-bed rectangle quartz reactor	94 ppmv benzene in oxygen, 20 mL/min	5-h reaction gave 72% benzene conversion and 190 ppmv CO₂ yield	[112]
Spray-coated polyester fibre supported non-metal doped TiO₂	Formaldehyde	30 W fluorescent lamp at 400–700 nm	A fixed-bed flow reactor	9 ppm HCHO at 1.0 L/min with 60% RH	Highest conversion rate of 38% at C-TiO₂	[124]

ous bacteria is not clear yet [97]. In this section we discuss the photocatalytic removal of H₂S by two routes, e.g. decomposition to produce hydrogen and PCO.

Based on a visible light photocatalyst of N-TiO₂/graphene, Bhirud et al. [98] described hydrogen evolution processes of photocatalytic decomposition of hydrogen sulfide.

$$H_2S + OH^-_{ads} \rightarrow HS^-_{ads} + H_2O \tag{51}$$

$$2HS^-_{ads} + 2h^+ \rightarrow 2S + 2H^+ \tag{52}$$

$$2H^+ + 2e^- \rightarrow H_2 \tag{53}$$

For air purification, PCO processes appear more feasible avoiding explosive hydrogen gas formation, which is the main interest of energy innovation. The final product of PCO of H₂S is sulfate, as described in below processes.

$$H_2S_{ads} + h^+ \rightarrow H_2S^+_{ads} \rightarrow HS^{\cdot}_{ads} + H^+ \tag{54}$$

$$^{\cdot}OH_{ads} + H_2S^+_{ads} \rightarrow HS^{\cdot}_{ads} + H_2O_{ads} \tag{55}$$

$$HS^{.}_{ads} + O_{2,ads} \rightarrow HSOO^{.}_{ads} \tag{56}$$

$$HSOO^{.}_{ads} + O_{2,ads} \rightarrow SO_{2,ads} \tag{57}$$

Then following the oxidation processes of SO_x, sulfate would be formed with the PCO removal of H_2S.

3. Photocatalysts for air purification

3.1. Overview of photocatalyst materials

Earlier studies on air purifications, for example PCO of VOCs and inorganic gas pollutants, were mainly carried out over wide band-gap semiconductor photocatalysts. The foundation of the PCO air purification providing the mechanism of removal processes was dependent on the surface reactions on TiO_2 and ZnO [3,87,92,99–101]. Only very few studies were conducted on other photocatalysts.

Once the mechanism and the applications of PCO for air purification are established, the critical aspects will be the developments of photocatalyst materials and the photocatalytic reactors. In this section, we focus on the development of materials. So far, photocatalysis has employed a wide variety of materials as the catalysts. For instance, metal oxides including binary compounds (TiO_2, ZnO, WO_3, Fe_2O_3, ZrO_2 etc), ternary compounds (vanadates, tantalates, tungstates, and bismutates, etc.), and other complex oxyhalides [102]. For the simple TiO_2 photocatalyst, there are immense modification techniques that have produced doped TiO_2 (Ti^{3+} self-doping, metal-doping, non-metal doping, and co-doping), dye-sensitized TiO_2, surface-modified TiO_2, mesoporous TiO_2, semiconductor-coupled TiO_2, shape-controlled TiO_2 (with preferred exposed facets), and supported TiO_2 [14].

In the studies on visible light photocatalysis, metal sulfides, nitrides and oxynitrides are also applied [103]. Based on surface plasmon effect of surface deposited noble metals, plasmonic photocatalysts were recently developed [20]. More recently, metal-free photocatalysts, represented by graphitic carbon nitride, also have attracted extensive attention in visible light photocatalysis [16,104].

It is almost impossible to give a comprehensive survey on the photocatalyst materials in PCO air purification. Alternatively, in this paper we hereby summarize the *latest three-year progress (2013–2015)* providing the most advanced photocatalysts for air purification.

3.2. TiO₂-based photocatalysts

3.2.1. PCO removal of VOCs

With the increasing concern of indoor air quality, VOCs as the main contaminants of indoor air pollution have become the most popular PCO targets [38,53]. With the development of novel photocatalysts for PCO, TiO_2 has been extensively investigated. Table 2 lists the selected results of TiO_2-based PCO for VOCs removal published in the last three years. Different from aqueous degradation, continuous reactors have been usually used for PCO removal of VOCs, including benzene, toluene, TCE, ethanol, acetone, acetaldehyde, formaldehyde, and others.

Size-dependence [105], shape-control [106], tailored porous structure [107] and preferentially exposed facets [108] are main parameters for manipulation of pure TiO_2 materials. As discussed above, PCO processes are based on the surface reactions facilitated by the formation of reactive radicals, therefore, the higher BET surface and pre-adsorption and more active surface would lead to a better PCO performance.

As other well-investigated photocatalysts, modification of TiO_2 has been found to be effective for a higher activity and a better stability in PCO air purification. Semiconductor coupling [109], transition metal doping [110], noble metal modification [111], and non-metal doping [112] have been employed for enhanced photocatalysis in PCO VOCs removal. It is noteworthy that in practical applications, material development and immobilization technique can be integrated. For example, Pham and Lee [113] prepared V-doped TiO_2 for enhanced photocatalytic activity. They also loaded the modified V-TiO_2 photocatalyst onto porous polyurethane, which was then applied in a continuous reactor for removal of toluene.

Table 2 strongly suggests that TiO_2-based photocatalysts are able to efficiently decompose a wide variety of organic compounds. With decades' research, it was concluded that pristine TiO_2 was required modification for enhanced photocatalysis. In recent studies, modified TiO_2 photocatalysts by means of doping, coupling, and shape-controlling were more frequently employed. Moreover, due to the consideration of scale-up of the gas-phase reactions, supporting materials or films were used for immobilization of the powder photocatalysts.

3.2.2. PCO removal of inorganic gas pollutants

Removal of inorganic gas pollutants, such as NO_x, SO_x, CO or H_2S is very important for both indoor and outdoor air purification. In comparison to VOCs removal, PCO studies in this field are less intensive. However, investigations on TiO_2-based studies are similar to the scope of PCO removal of VOCs. Table 3 lists the selected results in PCO removal of gas inorganic pollutants on TiO_2-based photocatalysts.

For a practical use, continuous reactors are always the first choice for air purification. Supported TiO_2 or its film will be able to provide a higher mechanical strength than powders. Anatase TiO_2 coatings were fabricated on electronspun polymeric nanofibers. It was found that the functionalized polyamide 6 and polystyrene nanofibers can be used as promising materials for NO conversion to NO_2 and HNO_3 [125].

It is well known that pristine TiO_2 can only respond to UV. For visible light photocatalytic NO oxidation, oxygen-deficient TiO_2 was prepared [126]. The absorption threshold was extended to visible light region enabling visible light NO removal. The roles of oxygen vacancies were studied by the first-principles density functional theory calculations, which confirmed the band gap narrowing and enhanced electron-hole separation rates.

Metal-doping has been widely used to design efficient TiO_2-based photocatalysts for PCO of inorganic gas pollutants. Ma et al. [127] reported that in visible light PCO of NO_x, Fe doping can extend the UV–vis absorption and improve the photoluminescence of TiO_2 for enhanced photocatalysis. Hu et al. [128] reported that in Pt/TiO_2, Pt^{4+} ions were doped into TiO_2 crystal lattice with part as PtO on the surface. Enhanced NO_x removal was observed due to the synergistic effect of two Pt species coexisting in the catalysts.

Coupling TiO_2 to another semiconductor is also an efficient strategy for tailoring the light absorbance and enhanced photocatalysis. In PCO of H_2S, a new function of coupling was reported by Alonso-Tellez et al. [129] It was suggested that coupling WO_3 to TiO_2 UV 100 (Hombikat) was not beneficial from semiconductor coupling. The ability of WO_3 lied in the delayed release of SO_2 to the gas phase for maintaining a weak selectivity into the unwanted SO_2 by-product.

Jiao et al. [130] applied a surface modification method to prepare a ternary photocatalyst of RuO_2/TiO_2/Pt with controlled the particle size of RuO_2 at ca. 2 nm. The developed photocatalysts were applied for enhanced PCO removal of CO under UV. It was found that the optimal RuO_2 modified TiO_2 provided 20, 15 and 8 times higher activity than P25, anatase and rutile TiO_2, respectively. The formation of interfacial epitaxial RuO_2 can lead to more

Table 3
Photocatalytic oxidation of inorganic gas pollutants on TiO_2-based photocatalysts.

Photocatalyst	Pollutant	Light source	Reactor	Reaction condition	Performance	Refs.
Polymeric nanofibers supported anatase TiO_2	NO_x	UV365 at 1.0 mW/cm^2	A tubular continuous reactor	1 ppm of NO in air with 50% RH	About 16% NO conversion	[125]
Oxygen-deficient TiO_2	NO	Visible light of 35.8 mW/cm^2	A continuous reactor	400 ppm NO with 55% RH at a flow rate of 1.2 L/min	About 75% NO removal	[126]
Fe/TiO_2	NO_x	Visible light (420–700 nm) of 35.8 mW/cm^2	A fixed-bed continuous reactor	400 ppb of NO at a flow rate of 1.2 L/min and with 55%RH	The conversion of NO_x (38%) was highest on the best sample of Fe0.1% T	[127]
Molybdenum-doped TiO_2 nanotubes	NO_2	UVA365 at 1.25 mW/cm^2	A continuous reactor	NO at 400 mL/min and 55% RH	77% NO_x removal	[131]
Pt-doped TiO_2	NO_x	UV 365 at 1.6 mW/cm^2 and visible light 420 nm at 0.7 mW/cm^2	A quartz rectangular reactor	NO in N_2 and wet air at around 40 ppm and 70%RH with a flow rate of 200 mL/min	0.4% Pt-TiO_2 showed around 30% NO conversion vs. 5% of P25 under visible light irradiations	[128]
Au/CeO_2-TiO_2	NO	UV or visible light	A continuous reactor	500 ppb of NO with 83% RH at a flow rate of 4.0 L/min	83% NO conversion vs. 48% over pure TiO_2	[132]
Dye-modified TiO_2	NO	A 300 W Xe lamp	A fixed-bed reactor	1000 ppm, 1000 ppm NH_3, O_2% at 500 mL/min	99% NO conversion with 99% N_2 selectivity	[133]
Cobalt imidazole complex functionalized GO supported TiO_2 film	NO_x and CO	UV of 3.0 mW/cm^2	A batch reactor	1 ppm NO_x and 50 ppm CO with 40% RH	Deterioration rate of 51% for NO_x and 46% for CO, higher than unmodified TiO_2 film	[134]
WO_3/TiO_2	H_2S	UV365 at 3.3 mW/cm^2	A two-coaxial tube reactor	15 ppm H_2S in and air (92%) and He at 200 mL/min	Best condition for 70% H_2S conversion and 60% sulfur removal on 5%WO_3/TiO_2	[129]
RuO_2/TiO_2/Pt	CO	UV of 1.0 mW/cm^2	A closed loop system	470 ppm CO	Best sample provide 100% CO conversion in 60 min	[130]
Multi-walled carbon nanotubes supported Cu/TiO_2	SO_2 and NO	UV365 of 0.65 mW/m^2	A continuous fixed-bed reactor	73 ppm NO and 155 SO_2 in 8% O_2 and 5% H_2O at 2 L/min	62% SO_2 removal and 43% NO removal	[135]

significant exposure of RuO_2(1 1 0) facets, which were believed to be the key factor for the improved PCO removal of CO.

3.3. Non-titania based photocatalysts for air purification

In spite of the enormous research activities on TiO_2-based photocatalysts, researchers never give up the exploration of novel photocatalysts. Table 4 lists a variety of novel photocatalysts that have been developed for PCO removals of either VOCs or inorganic gas pollutants.

ZnO is the second most popular semiconductor photocatalyst. In aqueous-phase photocatalytic reactions, it can show a higher activity than TiO_2, but the stability is not as good as TiO_2. In PCO air purification, ZnO has been also investigated. Liao et al. [136] modified the morphology (six prisms, short six pyramids and long six pyramids shape) and crystal defect of ZnO. The degradation efficiency of the modified ZnO was higher than P25 for formaldehyde removal, due to that the polar planes of the modified ZnO possess higher surface energy, which ensures a higher photocatalytic activity. A ZnO/graphene composite was prepared by a facile, green one-pot hydrothermal method for degradation of gaseous acetaldehyde [137]. The introduction of rGO (reduced graphene oxide) can increase the electron transfer rate so as to improve the photocatalytic activity. Therefore, a proper rGO content can significantly enhance the degradation rate and CO_2 generation.

Hematite α-Fe_2O_3 is the most stable iron oxide that possesses n-type semiconductor properties and a band gap energy of 1.9–2.2 eV, enabling it as a promising visible light photocatalyst. Sugranez et al. reported that α-Fe_2O_3 can be used for PCO removal of NO_x, following the processes of $NO \rightarrow NO_2 \rightarrow NO_3^-$ with retention of HNO_2/NO_3^-.

Besides single metal oxides, bimetal oxides were also developed as photocatalysts. For example, Huang et al. prepared a $Zr_xTi_{1-x}O_2$

photocatalyst and applied it for decomposition of gaseous HCHO [138]. Two narrow band gap semiconductors, Bi_2SiO_4 and AgI were coupled via an in situ precipitation method [139]. In PCO removal of formaldehyde, enhanced performance was observed compared to single Bi_2SiO_5, due to the presence of Bi_2SiO_5, AgI and metallic Ag which can cause the inner electric field originated from the exposure of (1 0 0) facets.

More recently, graphitic carbon nitride has become a very popular metal-free photocatalyst owing to the nature of polymeric semiconductor [13,104]. Sun et al. [140] reported that g-C_3N_4 nanosheets were deposited by Ag nanoparticles, which were then used for PCO removal of NO_x under visible light irradiations. It was found that Ag nanoparticles not only enhanced the activity, but lead to the selectivity of final products. Katsumata et al. [141] prepared g-C_3N_4/WO_3 composites and applied them for visible-light-driven photodegradation of acetaldehyde pollution. The optical absorption was determined by the energy range of 2.65–2.75 eV, as such visible light photocatalysis was ensured. The synergistic effect of g-C_3N_4 and WO_3 was proposed to be responsible for the enhanced photocatalysis.

A recent survey of the photocatalysts for PCO air purification shows that compared to other applications, such as aqueous degradation, CO_2 reduction, and hydrogen production, the exploration of novel materials is still highly desirable. The new photocatalyst materials for PCO air purification are far beyond satisfactory.

3.4. Immobilization techniques

The immobilization of TiO_2, i.e. Degussa P25, photocatalyst becomes a critical technique for fabrication of photoreactors for air purification. Two main strategies have been applied for immobilization of TiO_2 powders, (a) coating TiO_2 on supporting materials, and (b) fabricating TiO_2 as a film. Thevenet et al. [114]

Table 4
Photocatalytic oxidation of VOCs on non-TiO_2-based photocatalysts.

Photocatalyst	Pollutant	Light source	Reactor	Reaction condition	Performance	Refs.
Morphology and crystal defect controlled ZnO	Formaldehyde	UV of 3.6 mW/cm^2 and visible light of 35.5 mW/cm^2	A 1.2-L batch reactor	100 ppm formaldehyde	25% conversion	[136]
ZnO-graphene	Acetaldehyde	UV of 1.0 mW/cm^2	500 mL batch reactor	200 ppm initial concentration	1.6 times higher activity than pure ZnO	[137]
α-Fe_2O_3 (1.9–2.2 eV)	NO_x	0.25 mW/cm^2 UV and 58 mW/cm^2 visible	A continuous laminar reactor	100 ppb NO with 50% RH	20% removal	[142]
$MnFe_2O_4$ hollow nanospheres (1.61 eV)	Benzene	Visible light of 50 mW/cm^2	A batch reactor	280 ppm benzene	Effective degradation under visible light irradiation	[143]
$Zr_xTi_{1-x}O_2$	Formaldehyde	UV–vis	A batch reactor	1 ppm formaldehyde with 50% RH	Enhanced degradation than P25	[138]
Bi_2SiO_5 (3.54 eV)/AgI (2.76 eV)	Formaldehyde	Visible light	800-mL batch reactor	2 µL formaldehyde injection	Better than single component	[139]
$CdSnO_3 \cdot 3H_2O$ (4.4 eV)	Benzene, cyclohexane and acetone	UV	A continuous tubular quartz microreactor	280 ppm acetone at a flow rate of 20 mL/min	25% conversion	[144]
$MSn(OH)_6$ (M = Co, Cu, Fe, Mg, Mn, Zn)	Benzene	UV	A continuous plug flow micro-reactor	250 ppm benzene balanced with O_2	MgHS and ZnHS showed enhanced benzene oxidation than P25	[145]
$Ag/BaAl_2O_4$ (1.63 eV)	Toluene	UV of 0.042 mW/cm^2	A continuous photoelectrical cell	750 ppm toluene in 21.6% O_2 + 78% N_2 + 0.4%H_2O with a flow rate of 20 mL/min	Around 92% conversion on $Ag/BaAl_2O_4$ vs. 80% on P25	[146]
$BiOI/Al_2O_3$	NO and SO_2	Visible light of 6 mW/cm^2	A stationary Pyrex glass column reactor	Initial concentration of 2000 ppm	1.83% BiOI on Al_2O_3 for 100% conversion for both NO and SO_2	[90]
Ag/g-C_3N_4	NO_x	Visible light	A 4.5-L batch reactor	100 ppm NO in 2.4 L/min air and 15 mL/min NO with 50% RH	70% conversion vs. 50% conversion on g-C_3N_4 only	[140]
g-C_3N_4/WO_3	Acetaldehyde	UV of 1.0 mW/cm^2	A batch reactor	250 ppm of acetaldehyde with 50% RH	Higher conversion and CO_2 formation than single component	[141]
g-C_3N_4-$BiVO_4$	NO	Visible light	A fixed-bed continuous reactor	400 ppm No in 7% O_2 (N_2 balanced) at 100 mL/min	3–4 times higher than single component	[147]

loaded P25 TiO_2 onto glass fibres and applied them for PCO removal of acetylene. In the preparation, a dry mixture of 50 wt% colloidal silica (Snwtex colloidal silica) and 50 wt% TiO_2 (Degussa P25) was suspended in water for deposition onto silica glass fibres. Other porous or functional supports, such as monolith [115], graphene oxide [116], PVC sheets [117], or optical fibres [118], were also employed for immobilization of photocatalyst powders. Fabrication of TiO_2 film is also a powerful technique for immobilization of photocatalyst powders for air purifier. Xie et al. [119] employed a PVP (polyvinylpyrrolidone) modified sol-gel route to fabricate TiO_2 thin film on window glass. They found that in PCO removal of acetone and benzene, enhanced decomposition rates were observed due to the improved crystallinity in comparison to that derived from non PVP addition. Antonello et al. [120] applied a novel procedure by electrochemical assistance for fabrication of transparent and mechanically robust TiO_2 film, which was then employed for gas-phase PCO removal of VOCs. The film not only showed excellent performances for VOCs removal but appeared as a promising self-cleaning material.

The main methods of catalyst immobilization on a support are the sol-gel, thermal, chemical vapor deposition, layer-by-layer and electrophoretic deposition methods. Each method is briefly described below and has its own merits.

The sol-gel method is a simple method whereby the catalyst support (for example: glass plates or glass rings) are dipped at a controlled rate in a colloidal solution of the TiO_2 precursor followed by calcinations at high temperature (>450 °C). This method has been widely used due to the low cost and flexibility with a wide range of shapes [148–150]. Recently, a low temperature (<150 °C) hybrid sol suspension method was devised that could be applied to various substrates such as aluminum, stainless steel,

glass fibres, Al_2O_3 monoliths etc, and be used to prepare stable, thick and highly active photocatalytic layers from different commercial TiO_2 nanoparticles [151].

In the thermal method, the catalyst is directly sprinkled on the support followed by thermal treatment [148,152]. The performance of the catalyst however depends on the calcination temperature, which influence the physical properties of the TiO_2 (crystal phase, structure, BET surface area and oxygen adsorption capacity) [153].

In chemical vapor deposition (CVD), the support is exposed to a gaseous atmosphere of the catalyst precursor at high temperature, which decomposes at the support surface [148,154]. This method has been used to prepare N-doped TiO_2 from multiple precursors [155]. The method can also be used to control the film thickness [156] and provide in situ TiO_2 crystallization [157,158].

The layer-by-layer (LBL) method uses a colloidal solution of the catalyst precursor to dip or spray a few times on the support until a layer of the desired thickness is obtained. The catalyst is bound to the support electrostatically. In this method the catalyst thickness can be easily controlled and the nanoparticles are well dispersed within the porous matrix, hence providing a high surface area. Furthermore, a high calcination temperature is not required [154,159–161].

The electrophoretic deposition (EPD) technique uses the movement of charged particles in a stable suspension upon the application of an electric field. This method is environmentally friendly, provide controllable film thickness and can be used on complex shapes. EPD has been used on plastic substrate [162], inside the pores of TiO_2 nanotube array [163], to deposit chitosan/h-BN/TiO_2 composite coatings on metal [164] and could possibly be used to coat biological molecules in the future [165].

3.5. Photocatalyst design for PCO air purification

In addition to general requirements for photocatalysts, several parameters should be considered for developing novel photocatalysts for PCO air purification.
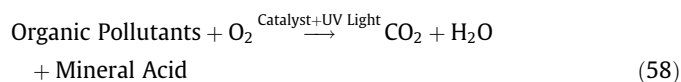
(a) Proper band structures for formation of reactive species. In the discussion of the purification processes, including VOCs degradation and oxidation of various inorganic gases, the formation of reactive radicals (·OH, ·O_2^-, HO_2, etc.) are essential for the oxidation processes. The proper valence band position (top of VB) for formation of ·OH (via hole oxidation) and conduction band position (bottom of VB) for production of ·O_{2ads}^- (via electron reduction) would be compulsory for the photocatalyst materials [104]. As the degradation of gaseous VOCs could be analogized to photodegradation of aqueous pollutants, therefore, the progress of material development might be beneficial to each other.

(b) Selectivity of the photocatalysts. In degradation of organic pollutants [166,167] in water or VOCs [168–171], the preferred products would be CO_2, H_2O and some inorganic compounds. The unwanted product in PCO removal of gaseous VOCs is coke that can deposit on the surface of the photocatalysts. In PCO removal of inorganic gas pollutants, selectivity is also important. For example, in NO_x removal, the physiochemical properties of a photocatalyst can lead to formation of N_2 or NO_3^- [50]. In removal of SO_x or H_2S, it is desirable to oxidize the compounds to SO_3/SO_4^{2-}, as formation of sulfur on the surface will block the active sites of the photocatalysts [88].

(c) Stability of the photocatalysts. The selectivity can partially influence the stability of the photocatalysts. In practical applications, a long-term stability is very important as the frequent replacement of the filter leads to high costs. In addition to the selectivity, the robust crystal structure, surface feature and chemical states are critical. Advanced surface modification can be considered for tailoring the selectivity and prolonging the stability [171].

(d) Visible light response. Visible light photocatalysis has attracted worldwide attention due to the implication of efficient solar energy. In outdoor air purification, it would be promising if an advanced reactor can be designed for solar energy utilization. In fact, this is more feasible than wastewater treatment, because in photodegradation of aqueous pollutants, the light diffusion by suspended particles is a critical design parameter [172,173]. In indoor air purification, visible light response of the materials also promises the prevention of bio-hazardous UV exposure and the possibility of the utilization of room lighting [171].

(e) Immobilization of the photocatalysts. It is seen that continuous reactors are frequently used in the air purification, which is different from photodegradation of organic pollutants in water. Continuous operation can be also implicated to real applications. Therefore, the immobilization of photocatalysts becomes a key technique in this field. Fabrication of photocatalyst film, incorporating the modification of composition or surface structure, can be one option. Also, porous supporting materials can be selected for improving the mechanic aspect of the photocatalysts. Advanced material design should also consider the simultaneous functionalization of the photocatalysts during the immobilization processes.

4. Design of gas-phase photocatalytic reactors

Gas phase photocatalysis is a process that uses the synergetic interaction of light, a semiconductor catalyst and an oxidizing agent (O_2 or H_2O) to decompose organic pollutants in air. Photocatalysis presents numerous advantages over its conventional counterparts such as adsorption or filtration. The organic pollutants are completely oxidized to CO_2 and H_2O, instead of being merely transferred from one place to another and therefore do not pose a disposal issue. The process is operated at ambient conditions, making it suitable for integration in existing heating, ventilation and air conditioning (HVAC) equipment [174]. Furthermore, photocatalysis works best at low concentration levels (ppb or ppm), which are the typical loading of polluted air in offices and buildings.

As explained in the previous sections, upon irradiation, the semiconductor catalyst generates electron-hole pairs. The holes can either directly oxidize adsorbed pollutants or can generate very reactive hydroxyl radicals ($OH^·$) from adsorbed water, which are powerful oxidants. The charge transfer loop is then closed with the remaining electron combining with O_2. The photocatalytic reaction can be summarized as follows:

$$\text{Organic Pollutants} + O_2 \xrightarrow{\text{Catalyst+UV Light}} CO_2 + H_2O$$
$$+ \text{Mineral Acid} \tag{58}$$

Photocatalysis has been widely studied for polluted air and wastewater treatment. However, in this paper, we will focus on the design and modelling of photocatalytic reactors for the treatment of volatile organic compounds (VOCs) in air.

This section presents some examples of the different types of photocatalytic reactors that exist. After that we present a section on the modelling of photocatalytic reactors, which is subdivided into hydrodynamics modelling, radiation transport modelling and finally kinetics modelling.

4.1. Types of gas phase photocatalytic reactors

Typically, VOCs are treated in photocatalytic reactors with the catalyst being immobilized on a surface. The generic laboratory scale photocatalytic reactors, designed for the determination of kinetic models, are the flat plate reactor and the annular reactor, with the catalyst immobilized on the reactor wall. Other reactor models are designed to have a high surface area of immobilized catalyst for intimate interaction between catalyst, VOC and radiation, hence achieving better performance and possible commercialization. Some examples are: monolith, packed bed and fluidized bed photocatalytic reactors for which some simplified representations are shown in Fig. 3. Several other types of photocatalytic reactors have also been designed such as corrugated plate [175], multi-annular [176], multi-plate [177], foam packed bed [178] and paper-based immobilized TiO_2 [179] reactor.

Each reactor geometry and design has its relevance. Plate type and annular type reactors are not designed for high air throughput and are therefore not commercialisable. However, they are of utmost importance in studies to determine kinetic parameters. Packed bed reactors are of simple construction and can have high conversion per unit mass of catalyst, however high radial radiation gradients can occur and the maintenance of the unit can be difficult. Fluidised bed reactors allow high throughput and low pressure drop, but are difficult to control and tend to suffer from catalyst losses in entrained air, which means that either catalyst replacement is needed or additional equipment such as cyclones could be required to separate and return the entrained catalyst to the reactor. Monolith type reactors are compact, have high throughputs and low pressure drops and could be easily incorporated in a HVAC system. However, the light intensity quickly declines through the monoliths. This could be solved by the use of individual optical fibres passing through each monolith, which could be challenging given the small pore size of the monolith
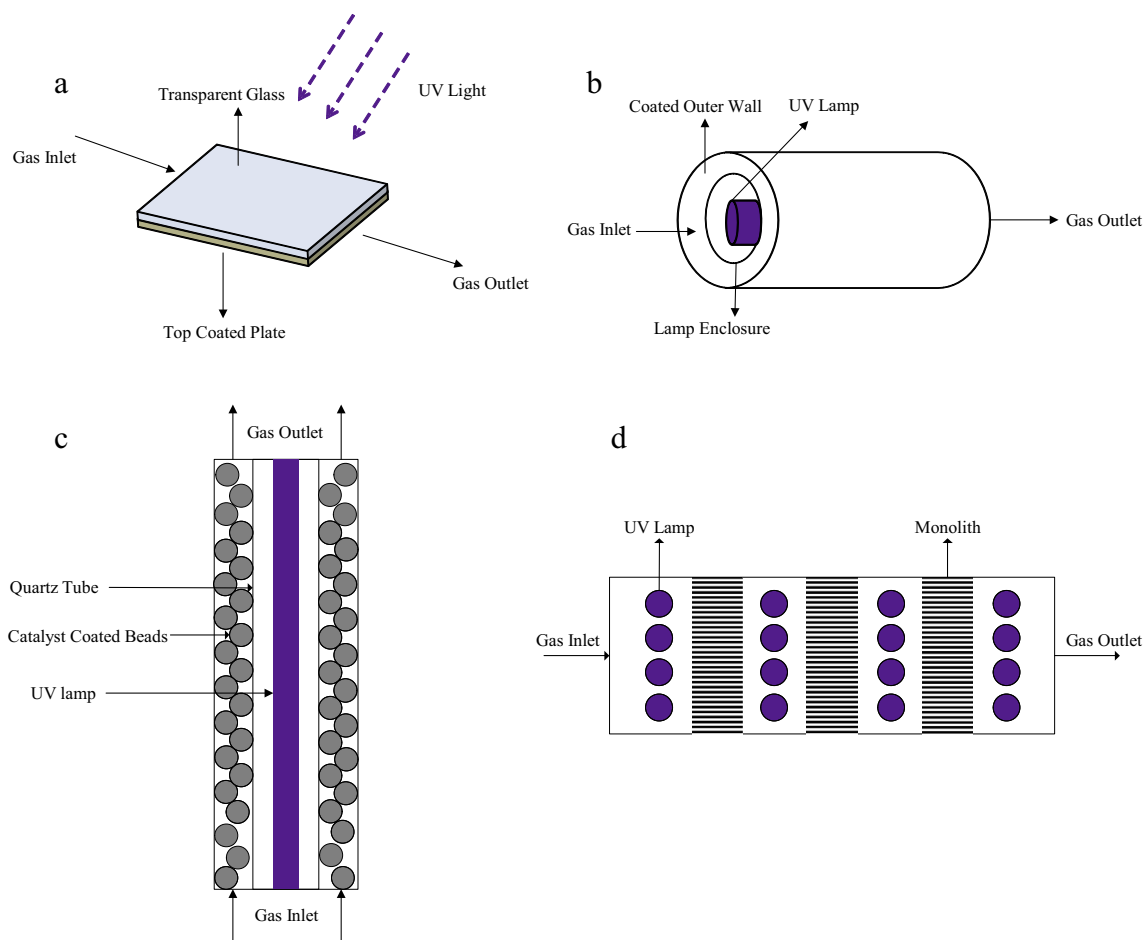
Fig. 3. Some types of gas-phase photocatalytic reactors: (a) coated plate, (b) annular, packed bed and (d) monolith (top view).

channels. Hence new reactor designs are required that can offer the best conditions for photocatalytic reactions, namely: compact size, large throughput, low pressure drop, optimal use of incident radiation, easy maintenance and reduced catalyst losses.

4.2. Intensification of photocatalytic reactors

The two main limitations in photocatalytic reactors are photon transfer and mass transfer. The design of new photocatalysts for the absorption of light in the visible spectrum is one option that has already been discussed in this paper. Alternatively, other process intensification techniques by means of novel configurations in light sources, reactor designs and optimal use of environmental conditions have been devised to overcome these limitations, which will be discussed here.

Light sources other than the conventional tubular lamps, such as optical fibres and LEDs act as miniature lamps and therefore offer better illumination in confined spaces. For example, optical fibres could be effectively inserted inside monolith channels for gas-phase photocatalytic reactions [180,181] to provide improved illumination efficiency, as opposed to surface illuminated monoliths that experience an exponential light decay through the monolith channels. Elsewhere, LEDs have been more commonly being used as an alternative light source in photocatalytic experiments [182–184] due to their higher efficiency in electricity-light conversion, small dimensions, robustness and long lifetime. Indeed, Doss et al. [183] found that visible light active TiO₂ MPT623/LED systems displayed energy effectiveness coefficients of about 50 times higher than that of TiO₂ P25/UV-A system.

Simple mechanical design alterations to annular reactors such as a single tangent inlet has exhibited better photocatalytic performance compared to basis reactor (normal inlet) or 6-winged baffle inlet reactor, due to spiraling flow over the catalytic wall, which improved contact time between pollutant and active surface [185]. Indeed, Destaillats et al. [186] showed that contact time was a critical parameter to be considered while investigating the performance of photocatalytic reactors under realistic conditions (i.e., large chamber, gas mixtures and low pollutant concentrations). They found that reducing the face velocity (hence contact time) in a flat plate reactor design improved pollutant degradation. However, if a reduction in air velocity was not feasible, the use of pleated media could significantly improve reactor performance by extending the contact time of pollutants on the irradiated surface. Otherwise, different reactor designs such as monolith channel type reactor provide a high surface area to volume ratio due to its honeycomb structure and also allow high flow rates with low pressure drop of the flowing air [115,187,188], meaning that as compact structures, they could be good potential candidates for scale-up. To further optimize the design of monolith reactors, Li Puma's group devised an overall monolith photonic efficiency factor (discussed in Section 4.4) for maximum photon absorption, that was dependent on dimensionless design parameters of the monolith reactor, from which they determined the optimal monolith aspect ratio, lamp-to-length ratio and optimal monolith-to-lamp-distance ratio [189]. The same factor was later used to optimize the design of a multi-plate photocatalytic reactor (MPPR) [177].

Under realistic environmental conditions, parameters such as light intensity levels, relative air humidity, pollutant concentration
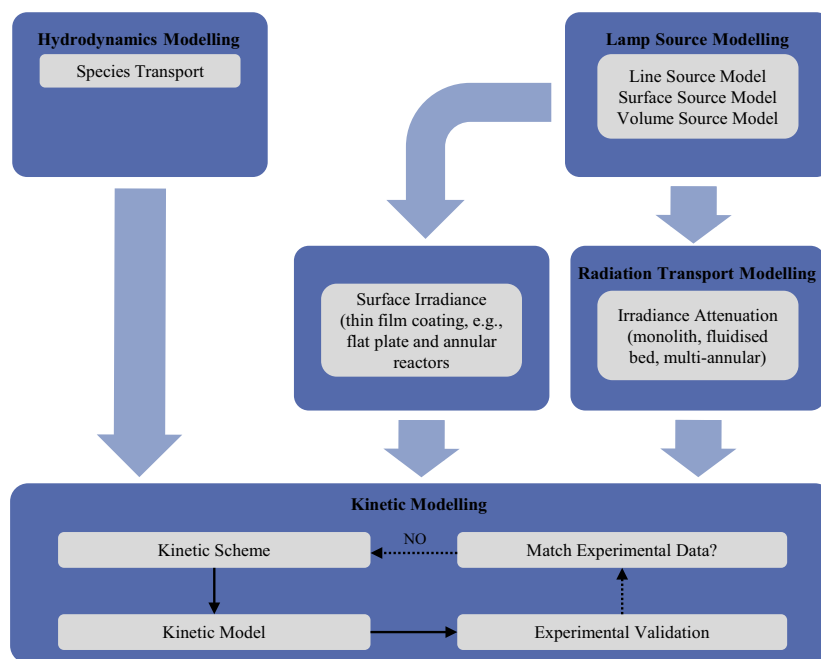
Fig. 4. Sequential steps in the modelling of gas-phase photocatalytic reactors.

and air flow rate (the latter having been previously mentioned) affect the photocatalytic rate. Depending on the type of pollutant used, the prevailing environmental conditions can be used advantageously for optimal photocatalytic degradation. For instance, NO_x photodegradation increased with increasing light intensity [190,191] and was more efficient under UVA rather than visible light [190]. Additionally, relative humidity could either positively or adversely affect the photodegradation rate. High percentages of relative humidity was detrimental to NO_x degradation at 20 ppmv concentration due to competitive adsorption of water and pollutant molecules on the photoactive surface [191], but resulted in higher conversion when the concentration was at 1 ppmv due to higher amount of hydroxyl radicals formed and non-competitive effects [190]. In another work, increase of relative humidity (15–60%) accelerated the photocatalytic degradation of toluene due to formation of hydroxyl radicals and participation of water molecules in the elimination of the accumulated intermediate benzaldehyde [192]. On the other hand, the oxidation rate of formaldehyde, 1,3-butadiene and toluene at sub-ppmv concentrations were found to increase with decreasing humidity for humidity levels above ca. 1000 ppmv [64]. Furthermore, humid air was found to be a good means for self-cleaning (catalyst regeneration) by assisting with the oxidation of carbon deposits formed during the decomposition of pollutants [193].

In regards to new technologies, non-thermal plasma (NTP) can generate high energy electrons at low energy input. Since these high energy electrons can ionize gas molecules to produce chemically active species, recent research has shown [194–196] that the combination of NTP with photocatalysis can provide a synergetic effect that is greater than the sum of each part, and therefore significantly improve the oxidation of pollutants in the treatment of polluted air.

4.3. Modelling of photocatalytic reactors

The modelling and design of photocatalytic reactors is significantly more challenging than that of conventional catalytic reactors due to the participation of radiation in chemical reactions.

The added intricacy occurs due to the dependence of the reaction rate with the local incident radiation intensity on the catalyst surface. Fig. 4 shows the sequential steps to be taken in the design of gas-phase photocatalytic reactors. Hydrodynamic modelling is required to determine the velocity, residence time and direction of the fluid. The local radiation incident on the catalyst surface can be found via an appropriate lamp emission model. If a high degree of light attenuation occurs in the direction of the fluid flow, then the amount of light absorbed by the catalyst can be calculated from the radiation transport modelling. With the knowledge of the fluid flow characteristics and the local light intensity/absorption, the kinetic modelling can be solved once an appropriate kinetic scheme has been developed. From the kinetic scheme, the intrinsic kinetic expression for a particular VOC can be derived. Each consecutive step presented in Figure will be described in the next sections of this paper.

4.3.1. Hydrodynamic modelling

Air flow within a photocatalytic reactor occurs at room temperature and pressure, which means that the air can be considered a Newtonian incompressible fluid with constant physical properties. The fluid and pollutant species mass balance can be solved from the classical continuity, Navier-Stokes and species conservation equations, respectively (Eqs. (59)–(61)) [197,198]:

$$\nabla \cdot (\rho v) = 0 \tag{59}$$

$$\nabla \cdot (\rho v v) = -\nabla P + \nabla \cdot (\tau) + \rho g + S_M \tag{60}$$

$$\nabla \cdot (\rho v C_i) = -\nabla \cdot J_i + r_i \tag{61}$$

where ρ is the density, v is the velocity vector, P is the pressure, τ is the viscous stress tensor, g is the gravitational constant, C_i is the molar concentration of species i, J_i is the diffusion flux of species i and r_i is the rate of consumption of species i, respectively. For monolith type reactors, Eqs. (59)–(61) have been modified to include the porosity of the monoliths [198,199]. The term r_i in Eq. (61) stands for homogeneous volumetric reaction, which has been considered to occur in the case of monolith type reactors
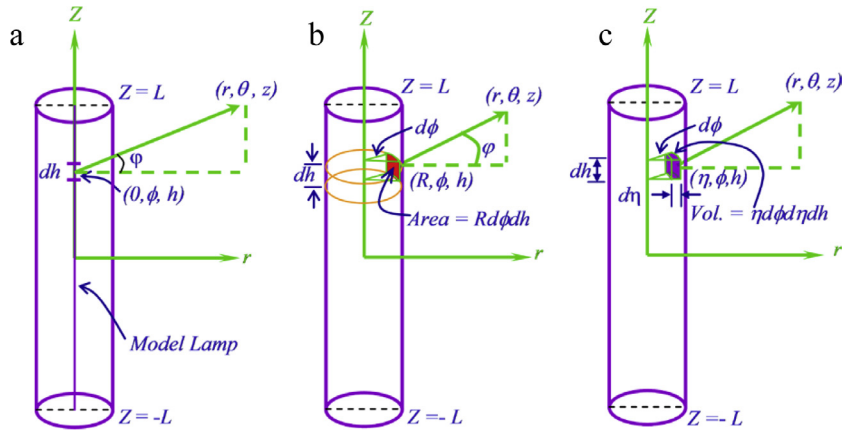
Fig. 5. Lamp emission models: (a) line source model, (b) surface source model and (c) volume source model [212].

[198,199]. However, in other types of reactors, reactions occur at the catalyst surface only and therefore r_i should be included in Eq. (61) when solving the species balance at the catalytic walls only, i.e., as a boundary condition. The term S_M in Eq. (60) is the momentum sink, implying loss of momentum due to an obstacle. Some correlations for S_M have been routinely used to account for momentum loss in monolith channels [198,199] or in perforated plates and photocatalyst supports [200,201].

To avoid the complexity of the mass transport equations, some approximations regarding the flow pattern inside reactors have been often utilized. Some authors performed 2D models and neglected diffusive flux in the axial direction compared to the convective flow [202]. When the size of the reactor is small, as for example, a laboratory scale reactor, and the volumetric flow rate is high enough so that mass transport limitation of pollutant species from the bulk to the catalyst surface is small, the plug flow model could appropriately describe the flow in the reactor [99,171,203–206]. The addition of a laminar velocity profile instead of fixed velocity could further improve mass transport description [207,208]. In another research [209], to approximate at best the flow in a non-ideal packed bed tubular reactor, an axial dispersed plug flow model was used. In this model, diffusion/dispersion processes that mix elements are superimposed on the convective flow in the axial direction and the dispersion term of the molar flow rate is formulated by analogy to molecular diffusion. Nevertheless, a correct description of the hydrodynamics is essential to capture fluid mixing, diffusion and reaction at the catalyst surface and therefore allow for a proper determination of the reaction rate. This is even more relevant when the reactor size is large such that the sum total effect of fluid elements having different velocities and directions cannot be ignored anymore, as will be discussed later.

4.3.2. Lamp emission models

The rate of a photocatalytic reaction depends on the intensity of the incident light reaching the catalyst surface. Hence an accurate determination of the local incident light flux impinging the catalyst surface is required. Photocatalytic reactors are normally illuminated by UV lamps that are located at an optimum distance to the catalyst film for maximum reaction. The calculation of radiant flux from a UV lamp at a certain point (r, θ, z, in cylindrical coordinates) on a catalyst surface depends on the type of lamp emission model used. The mathematical derivation of lamp emission models stems from the geometrical consideration of the emitting body. Consequently, 3 main models have been proposed, namely: the line source model, the surface source model and the volume source model, which are mathematically depicted in Fig. 5. The derivation

of the models can be found elsewhere [210,211] and are summarized in Eqs. (62)–(66). For the line and surface source models, light can be emitted either specularly or diffusely.

Line source specular emission : E_λ

$$= \frac{K_{\lambda 1}}{4\pi} \int_{-L}^{L} \frac{dh}{(r^2 + (z-h)^2)} \tag{62}$$

Line source diffuse emission : E_λ

$$= \frac{K_{\lambda 1}}{4\pi} \int_{-L}^{L} \frac{r\,dh}{(r^2 + (z-h)^2)^{3/2}} \tag{63}$$

Surface source specular emission : E_λ

$$= \frac{K_{\lambda 2}}{4\pi} \int_{h=-L}^{h=+L} \int_{\phi=-\pi/2}^{\phi=+\pi/2}$$
$$\times \frac{R\,d\phi\,dh}{[(r\cos\theta - R\cos\phi)^2 + (r\sin\theta - R\sin\phi)^2 + (z-h)^2]} \tag{64}$$

Surface source diffuse emission : E_λ

$$= \frac{K_{\lambda 2}}{4\pi} \int_{h=-L}^{h=+L} \int_{\phi=-\pi/2}^{\phi=+\pi/2}$$
$$\times \frac{\cos\varphi R\,d\phi\,dh}{[(r\cos\theta - R\cos\phi)^2 + (r\sin\theta - R\sin\phi)^2 + (z-h)^2]} \tag{65}$$

Volume source emission : E_λ

$$= \frac{K_{\lambda 3}}{4\pi} \int_{h=-L}^{h=+L} \int_{\eta=0}^{\eta=R} \int_{\phi=-\pi}^{\phi=+\pi}$$
$$\times \frac{\eta\,d\eta\,d\phi\,dh}{[(r\cos\theta - \eta\cos\phi)^2 + (r\sin\theta - \eta\sin\phi)^2 + (z-h)^2]} \tag{66}$$

where $K_{\lambda 1}$ = rate of photons emitted per unit length of lamp, $K_{\lambda 2}$ = rate of photons emitted per unit surface of lamp and $K_{\lambda 3}$ = rate of photons emitted per unit volume of lamp.

On the other hand, light emitting diodes (LEDs) are another type of light source that have high energy efficiency, long lifetime and compact sizes and they have recently found common use as light source in photocatalytic reactors [118,171,213–215]. A simple derivation of the equation for the incident radiation from an array of LED lamps on a flat catalytic surface is presented elsewhere [214].

There is no common agreement among researchers on which lamp model to use. The surface and volume source models consider the complete lamp dimensions as being emitting but can be

mathematically intensive. The Brandi, Alfano and Fernandez-Garcia groups, who have largely contributed to the field of photocatalytic reactor engineering, have consistently used the surface source model [175,176,202,216–218]. However, despite its mathematical simplicity, the line source model has been found to match very closely the volume source model [173,219] and has been preferred by many researchers [172,204,219–221].

It is important to realize that light emitted from a source normally passes through a quartz or glass envelope before reaching the catalyst surface. Research has shown that the effects of reflection and refraction through the envelope can be non-negligible [173,219,222,223] and should be considered in the modelling of incident radiation flux.

4.3.3. Radiation transport modelling

The radiative transfer equation (RTE) describes the movement of a bundle of light rays travelling in the direction s and having solid angle Ω, intensity I and wavelength λ. During its trajectory through a medium, the light will experience absorption, out-scattering and in-scattering. The RTE for an elemental distance ds is [212]:

$$\frac{dI_\lambda(s,\Omega)}{ds} = -\kappa_\lambda I_\lambda(s,\Omega) - \sigma_\lambda I_\lambda(s,\Omega) + \frac{1}{4\pi}\sigma_\lambda \int_0^{4\pi} p(\Omega' \\ \rightarrow \Omega)I_\lambda(s,\Omega')d\Omega' \tag{67}$$

where the first term on the right hand side is the absorbed radiation, the second term is the out scattering of radiation and the third term is the gain of energy due to in-scattering of radiation. The parameters κ_λ and σ_λ are the wavelength dependent absorption and scattering coefficients of the medium and $p(\Omega' \rightarrow \Omega)$ is a phase function describing incoming incident radiation from all other directions surrounding ds.

The RTE is not applied to the polluted air medium as it is transparent (no absorption) and does not scatter light. However, light is indeed absorbed through the catalyst film. Since the particles in the film are close together, the effect of absorption is much higher than scattering and Eq. (67) can be greatly simplified to an analytical form known as the Beer-Lambert law, Eq. (68):

$$\frac{dI_{0,\lambda}(s)}{ds} = -\kappa_\lambda I_{0,\lambda}(s) \tag{68}$$

where $I_{0,\lambda}$ is the incident radiation minus the reflected portion of radiation and the absorption coefficient is assumed invariable with distance s:

$$I_{0,\lambda} = I_{in,\lambda} - I_{ref,\lambda} \tag{69}$$

Due to the thin film thickness in coated photocatalytic reactors of the flat-plate or annular design and the assumption of intra-particle mass transport resistance through the film, surface reaction and therefore surface incident light flux has been taken into

consideration by most researchers. For these cases, solving the RTE is not required and the incident light reaching the catalyst surface can be calculated via the lamp emission models.

On the other hand, some reactor designs do experience an attenuation of light intensity with position such that the local light intensity has to be calculated. Some examples are fluidized bed reactors [224], monolith reactors [198,199] and multi-annular reactors [176,217]. The RTE should also be solved for packed bed reactors. Lopes et al. [209] used an average irradiance in the calculation of the reaction rate in a packed bed reactor. Although their model matched experimental data, the authors recognized the limitations of their model for not considering the radial variation of light intensity through the catalyst bed due to absorption and scattering.

Other methods have also been used to calculate radiation transfer. Some examples are an embedding technique which was used to find the light absorption by two outwardly illuminated CeO_2 films separated by a glass plate [216] and the Kubelka-Munk model that described light propagation within nano-TiO_2 immobilized paper sheets [179].

4.3.4. Kinetic modelling

At steady state, the photocatalytic reaction rate depends upon the surface coverage of the pollutant molecules on the catalyst particles. Therefore, it seems reasonable that the kinetic modelling of photocatalytic reactors is related closely to adsorption models. In this respect, the Langmuir-Hinshelwood (LH) relationship has been widely used in the literature. The LH model is usually modified to account for the effect of local light intensity in photocatalytic reactors:

$$-r_p = [I(x,y,z)]^n \frac{kKC_{p,s}}{1 + KC_{p,s}} \tag{70}$$

where k is the apparent rate constant, K is the Langmuir adsorption equilibrium constant and $C_{p,s}$ is the pollutant concentration at the catalyst surface. In the absence of mass transfer limitations, the pollutant concentration at the surface is equal to that in the bulk fluid. Absence of mass transfer is normally pre-determined by researchers and it occurs when the reaction rate becomes independent of the volumetric flow rate of the air in the reactor. Nevertheless, simplified models that account for the combined effect of mass transfer (from semi-empirical correlations) and photocatalytic reaction rate in reactors with constant cross-sectional areas have been presented elsewhere [225,226]. The exponent n in Eq. (70) depends on the incident light intensity. High incident intensity tends to favor the electron-hole recombination process ($n < 1$) while low light intensity favors pollutant degradation ($n = 1$). Some values of n for different pollutants and incident light intensities are presented in Table 5.

When the pollutant concentration is very small, Eq. (70) has been reduced to [174,228]:

Table 5
Value of n in some gas-phase photocatalytic reactors.

Pollutant	C_0	Reactor type	λ (nm)	Catalyst	E_w (W m^{-2})	n	Refs.
Trichloroethylene	25.1 μM	Flat plate	324–400	P25	⩽28.1	1	[220]
n-Decane	73–138 ppm	Annular monolith	280–400	PC500	18.9–38.4	0.8	[227]
Dimethylsulfide	3 ppm	Flat plate	365	P25	0–10	0.78	[171]
					10–25	0.16	
			375		0–10	0.69	
					10–25	0.2	
			385		0–25	0.75	
			402		0–25	0.86	
Ozone	8.687 ppm	Flat plate	365 ± 25	P25	2.5–10	0.6118	[204]
					10–25	0.1009	

$$-r_p = [I(x,y,z)]^n k' C_{p,s} \tag{71}$$

The LH model has been expanded to accommodate the effect of competitive water vapor adsorption to yield 3 main types of equations: LH bimolecular competitive one type of sites, LH bimolecular non-competitive two types of sites and LH bimolecular competitive two types of sites, Eqs. (72), (73) and (74), respectively [209,226,227,229,230].

$$-r_p = [I(x,y,z)]^n k \left(\frac{K_p K_w C_p C_w}{\left(1 + K_p K_w C_p C_w\right)^2} \right) \tag{72}$$

$$-r_p = [I(x,y,z)]^n k \left(\frac{K_p C_p}{1 + K_p C_p} \right) \left(\frac{K_w C_w}{1 + K_w C_w} \right) \tag{73}$$

$$-r_p = [I(x,y,z)]^n k \left(\frac{K_p C_p}{1 + K_p C_p + K_w C_w} \right) \left(\frac{K'_w C_w}{1 + K'_p C_p + K'_w C_w} \right) \tag{74}$$

where subscripts p and w refer to pollutant and water, respectively. Eqs. (70)–(74), while providing a satisfactory fit within the experimental ranges and for the specific reactor design investigated, are not representative of the true reaction processes occurring at the surface of the catalyst. Consequently, some authors could not match their experimental data with the LH models, once they used different operating conditions or reactor designs. For example, discrepancies were observed when the kinetic model of formaldehyde photodegradation performed in a glass plate reactor [231] was used on monolith type reactors [198,199].

A true representation of a reaction kinetic equation should contain intrinsic parameters, i.e. parameters that are independent of reactor geometry, radiation field and fluid dynamics. The intrinsic kinetic model is usually derived from a postulated, yet simplified kinetic scheme involving the different species taking place in a reaction. Passalia et al. [202] investigated the degradation of formaldehyde on a single pass flat-plate photocatalytic reactor. The intrinsic kinetic model was derived from a plausible reaction pathway that applied a kinetic steady state approximation for the net generation rates of radical species as well as electrons and holes. The reaction rate model could successfully replicate the experimental results obtained on a corrugated plate photocatalytic reactor [175,197,232]. Imoberdorf et al. [208,233] used a laboratory scale flat plate reactor to derive the intrinsic kinetic expression for the degradation of perchloroethylene (PCE), using previously published plausible mechanistic sequence involving chlorine radical attack of the PCE. The rate expression could be successfully used to model PCE degradation in multi annular photocatalytic reactors [176,217]. Using the same scheme as for PCE degradation, Li Puma et al. [229] derived a similar expression for trichloroethylene (TCE) degradation. Unlike the other proposed LH models in literature for TCE degradation, they showed that their model could explain the effect of water vapor concentration on the photocatalytic rate. Another expression for TCE degradation, albeit without the presence of water vapor, was obtained by explicitly taking into account electron-hole pair reactions, linear TCE adsorption/desorption equilibrium, first order reaction kinetics and steady state concentrations of holes and adsorbed intermediates [205]. Similarly from proposed reaction schemes, the intrinsic expressions for the photodegradation of cyclohexane [234] and toluene [218] have been proposed. For the sake of precise scientific and engineering practice, it is therefore imperative that future work in this field concentrate on the derivation of intrinsic kinetic expressions from possible reaction mechanisms.

4.4. Photocatalytic reactor performance

Reactor performance parameters are important to compare among different reactor configurations. The performance parameters should be independent of the operating conditions, reactor geometry and catalyst nature.

The most utilized performance parameter is the apparent quantum yield [185,202,220,235,236]. The apparent quantum yield is the ratio of the overall reaction rate to the overall amount of photon absorbed:

$$\Phi_{overall} = \frac{\langle r_p \rangle}{\langle e^{a,s} \rangle} \tag{75}$$

where $e^{a,s}$ is the local superficial rate of photon absorption (LSRPA).

Serrano and de Lasa [237] on the other hand suggested a photochemical thermodynamic efficiency factor (PTEF) for photocatalytic air treatment units as a parameter relating the energy utilized for hydroxyl radical formation over the irradiated energy on the photocatalyst.

Singh et al. [189] suggested the evaluation of two dimensionless parameters for the evaluation of monolith photocatalytic reactor performance: the monolith photon absorption efficiency (ϕ), which is the ratio of photons absorbed by the catalyst in the monolith divided by the photons emitted by the lamps and the factor that gives the uniformity of irradiation of the front surface of the monolith (η). From these two factors, the monolith overall photonic efficiency (Φ) can be calculated:

$$\Phi = \phi \eta \tag{76}$$

Imoberdorf et al. [176,238] defined the total quantum efficiency (η_T) to compare how well photocatalytic reactors make use of the energy emitted by the lamp to decompose the pollutant. η_T can be expressed as the product of the reactor radiation incidence efficiency (η_I), the catalyst radiation absorption efficiency (η_A) and the overall reaction quantum efficiency (η_R). The concept of multiple efficiencies was also used by Passalia et al. [232] for the performance determination of their corrugated-wall photocatalytic reactor.

For photocatalytic reactors of constant cross sectional area, Yang et al. [225] developed a number of transfer units (NTU) approach to determine the reaction effectiveness (η). Calculation of η could show if the reaction was mass transfer controlled, reaction controlled or in-between.

5. Modelling methods for gas-phase photocatalytic reactors

The main methods of photocatalytic reactor modelling are presented in this section, namely: Monte Carlo method, numerical methods and computational fluid dynamics.

5.1. Monte Carlo (MC) method

The MC method is a statistical technique that allows the tracking of individual photons. The emission of photons is stochastically defined and assigned random directions. The MC method takes into account the complex optical laws involved, such as refraction, reflection and absorption, whereby a Russian roulette algorithm is used to determine whether a photon hitting a wall is either absorbed or reflected. Being a statistical method, better solutions are acquired with higher number of virtual photons. The MC method is relatively simple to implement and is best useful when a high packing density of the catalyst is used (which is difficult to solve via other methods), such as monoliths [189], fixed bed [239,240], and packed bed [241] photocatalytic reactors. The MC method was used to predict the effect of the geometric shape (cir-

cular, square and triangular) of monolith channels on the radiation distribution [242]. In a recent study [198], the light distribution in a single channel of a monolith was modelled via MC so as to estimate its absorption coefficient, which was eventually used as an input parameter for the CFD modelling of the monolith reactor. In another work, the optimum reactor configuration of a multiple-plate photocatalytic reactor illuminated with one or multiple lamps was solved by MC method [177]. The optimal design was validated through experimental verification.

5.2. Numerical methods

Numerical methods use different computer based algorithms to solve the solution of sets of differential equations that are otherwise impossible to solve analytically. Numerical methods have been used to determine kinetic parameters from proposed LH models [229], to calculate the radiation field interaction between catalyst films [216,232] or in monolith channels [243,244] and to solve the mass, momentum, radiation and kinetic expressions [176,179,202,208,209,217,218,224,227,233,245–248] in photocatalytic reactors.

Imoberdorf et al. [208] used a non-linear regression procedure (Levenberg-Marquardt method) to find the kinetic parameters of an intrinsic kinetic model for PCE degradation in a laboratory plate photocatalytic reactor. The kinetic model could be used to predict the experimental data from a larger multi-annular reactor. In another work, non-linear least squares regression function was used [229] to fit the experimental data of the photocatalytic oxidation of TCE with five published kinetic models (one power law model and 4 LH models) for TCE degradation. It was found that the models did not fit the experimental data with respect to water vapor concentration. The authors then derived a kinetic model from a plausible kinetic scheme. The proposed model was apt at representing experimental data over all investigated TCE concentrations and could also replicate the effect of water on reaction rate.

Multiple reflections, absorption and transmission of radiation in a photocatalytic reactor consisting of outwardly illuminated TiO_2 thin films separated by a glass plate was solved numerically from an expression that combined a surface lamp emission model with the diffuse transmittance and reflectance of the different media [216]. In another work, a Gauss-Siedel method was used to calculate the incident radiation on the surface of a corrugated-wall photocatalytic reactor made up of triangular channels [232]. The effect of interchange of radiation between the walls was achieved through the use and computation of local view factors.

Hossain et al. [248] developed a rigorous 3D model from first principles for calculating the convection, diffusion and reaction in a square-channel monolith photocatalytic reactor. The model equations, consisting of a set of partial differential equations were solved via a numerical finite difference scheme based on the vorticity-velocity method. Imoberdorf et al. [217] developed a FORTRAN code to solve the radiation absorption field and mass balance with reaction in a multi-annular reactor. The model could also be used to determine the optimum configuration for multi-annular arrangement [176]. More recently, numerical methods have been successfully applied to a continuous-flow tubular reactor [209], annular reactor surrounded by 4 lamps [218], fluidized bed reactor [247], paper-based nano-TiO_2 immobilized on porous silica reactor [179] and combined photocatalytic and non-thermal plasma annular reactor [245].

5.3. Computational fluid dynamics (CFD)

CFD is a powerful tool that allows researchers to solve the hydrodynamics and radiation transport in photocatalytic reactors.

In a CFD software, the geometry of the reactor is reproduced with its exact dimensions. The geometry can then be meshed or subdivided into small elements and the transport equations (Eqs. (59)–(61)) can be solved for each individual element. In using small volume/area elements of the reactor where the fluid flows, the differential form of the equations is approached and a realistic solution of the hydrodynamics is therefore reproduced. CFD is particularly useful when the reactor sizes are relatively big and ideal flow cannot be assumed. Consequently the spatial accuracy of dead zones, recirculation zones, velocity fields and concentration fields can be properly captured. In setting up a case, the CFD user needs to specify known parameters such as physical parameters as well as boundary conditions such as inlet flowrate, species concentrations and outlet flowrate or pressure. Additionally, CFD can be used to solve the RTE via the discrete ordinate model (DOM). Analogous to the mass transport equations, the DOM discretises the volume elements into a number of directions for which the RTE is solved individually. CFD has been used to model photocatalytic reactors of various sizes and designs such as a corrugated plate [175,197,232], slit-shaped flat bed [174], narrow-slit flat plate [214], 6-winged baffle and tangent inlet annular [185], rectangular and cylindrical [249], annular [203,250,251], flat plate flow through [204,220,252], monolith [198,199], photo-CREC [201] and air purifier apparatus [253].

A corrugated plate photocatalytic reactor of 1.8 L volume for the oxidation of formaldehyde was modelled by CFD [175,197]. The radiation field was evaluated and introduced externally and the velocity and concentration fields were evaluated by CFD from intrinsic kinetic parameters obtained previously on a laboratory scale reactor. Simulations showed that the effect of catalytic walls was appreciable along each channel and a mixing effect was observed due to the change in direction from one channel to another. Good agreement was found between experimental data and simulated results with a root mean square error lower than 4%. CFD studies could also be performed to determine the effect of different folding angle of the triangular channels on the performance of a corrugated reactor of smaller volume [232]. In another work, a monolith type reactor was modelled by simulating the channels as porous zones [198]. The absorption coefficient of the channel was obtained independently by a MC method and used as a parameter in the radiation modelling. Although good agreement between experimental and simulated results for formaldehyde degradation was obtained, some discrepancies still existed which the authors attributed to a temperature effect. However, it is possible that the inconsistencies resulted from the usage of a non-intrinsic kinetic equation. The modelling of a slit-shaped flat bed photocatalytic reactor for acetaldehyde oxidation [174] was performed by a semi analytic method considering mass transfer and a CFD approach for comparison. It was found that the CFD approach could accurately calculate the spatial variation of flow rate, reaction rate and concentrations at the reactive surface, which could not be accounted for by the analytic mass transfer approach.

The effect of reactor design on performance can also be analyzed by CFD. For an annular type reactor, it was found that a simple modification from middle inlet to single tangent could make the stream flow in a whirlpool manner and improve the contact of the fluid with the catalyst wall, even when compared to a baffled inlet design [185]. In another work [201], the superiority of cylindrical cross-sectional design compared to a square one for a photo-CREC reactor was demonstrated due to improved fluid and radiation distribution on the catalyst surface.

The intrinsic kinetic parameters for the photocatalytic oxidation of TCE in a flat-plate reactor could be found with a high degree of confidence by 3D CFD modelling [220], since the model considered the actual flow pattern, non-uniform radiation incidence on the catalytic plate and the effect of the concentration of the reactant.

The same authors later showed that a simple 2D model could very well approach the predictions from the 3D model [252], which greatly simplified implementation and computation time. In a different work [249], CFD studies were performed on a rectangular reactor to determine the intrinsic reaction rate constants for ethylene degradation. The constants found from CFD were much higher than the ones determined analytically (i.e. by assuming plug flow) due to the largely non-ideal flow occurring in the reactor. Nevertheless, when the CFD determined constants were applied on a reactor of cylindrical design, the simulated results matched very well the experimental data.

Difficulties may arise in CFD modelling when the boundary conditions are not known or properly set up. Indeed, in the modelling of a photocatalytic air purifier for acetaldehyde removal [253], a lack of accuracy between experimental and modelling results was observed due to the difficulty in evaluating the precise outlet velocity from the apparatus to set an accurate value of the total pressure lost through the fans.

6. Outlook and conclusions

The tremendous amount of work invested in the design of photocatalysts and photocatalytic reactors within the past years demonstrate the belief in this process becoming a future treatment method for polluted air. Great progress has been achieved in the understanding of the mechanism of pollutant degradation, light absorption and charge separation so that catalysts are now being tailored to achieve even better performances. However, despite the advances, photocatalysis will still not be viable for commercialization until recurrent issues such as low quantum efficiency, visible light absorption capability, selectivity towards CO_2 and H_2O production and stability are addressed. This will require contributions from a variety of specialised groups such as band gap engineers, material scientists, chemical engineers and chemists. As such, the doping of well-known semiconductors such as TiO_2 and ZnO with metals, metal oxides or non-metals such as carbon or carbon nitrides as well as the use of composites and perovskite-based materials would be a step in the right direction. In the reactor design, new concepts will be required that increase the surface area of photocatalyst that is in contact with light and achieve a low pressure drop of the flowing gas. Intrinsic kinetic models will need to stem from viable degradation mechanisms, depending on the pollutant used so that they can be used for a range of conditions and reactor types. Computational models, which are derived from fundamental transport equations, have been shown to be powerful tools for the experimental validation of various types of reactors. Nevertheless, the knowledge of fluid flows is essential for the proper design of photocatalytic reactors and therefore, CFD based models are of utter importance, above all when the reactor is of considerable size. Furthermore, more studies carried out at the more realistic ppb levels, due to the difficulty at generating and controlling such low concentrations, are required and the effect of gas mixtures, which will entail more complicated degradation mechanisms and reaction kinetics will have to be investigated. Finally, a set of international standards are required for photocatalytic products so that comparison can be made among products from different producers via simple tests. The current ISO standards (ISO 22197: test methods for air-purification performance of semiconductor photocatalytic materials) have been set up for 3 common pollutants: NO, acetaldehyde and toluene [254]. However, different, expensive and complicated analytical equipment are required for each test and the preconditioning treatment is inconsistent for each standard [255]. Setting up of similar protocols for all pollutants have been suggested in terms of experimental procedures and data analysis while published standards for other common pollutants such as formaldehyde and methyl mercaptan are required and pending [255]. Therefore, a lot of challenges and concerns still remain to be addressed in the exciting field of photocatalysis before this technique becomes viable for commercialisation.

References

[1] A. Fujishima, K. Honda, Electrochemical photolysis of water at a semiconductor electrode, Nature 238 (1972). 37-+.
[2] A.J. Bard, Photoelectrochemistry and heterogeneous photocatalysis at semiconductors, J. Photochem. 10 (1979) 59–75.
[3] R.I. Bickley, G. Munuera, F.S. Stone, Photoadsorption and photocatalysis at rutile surfaces. 2. Photocatalytic oxidation of isopropanol, J. Catal. 31 (1973) 398–407.
[4] T. Inoue, A. Fujishima, S. Konishi, K. Honda, Photoelectrocatalytic reduction of carbon-dioxide in aqueous suspensions of semiconductor powders, Nature 277 (1979) 637–638.
[5] S. Yamagata, S. Nakabayashi, K.M. Sancier, A. Fujishima, Photocatalytic oxidation of alcohols on TiO_2, Bull. Chem. Soc. Jpn. 61 (1988) 3429–3434.
[6] B.C. Faust, M.R. Hoffmann, D.W. Bahnemann, Photocatalytic oxidation of sulfur-dioxide in aqueous suspensions of alpha-Fe_2O_3, J. Phys. Chem. 93 (1989) 6371–6381.
[7] E.C. Butler, A.P. Davis, Photocatalytic oxidation in aqueous titanium-dioxide suspensions – the influence of dissolved transition-metals, J. Photochem. Photobiol. A 70 (1993) 273–283.
[8] R. Wang, K. Hashimoto, A. Fujishima, M. Chikuni, E. Kojima, A. Kitamura, M. Shimohigoshi, T. Watanabe, Light-induced amphiphilic surfaces, Nature 388 (1997) 431–432.
[9] A.L. Linsebigler, G.Q. Lu, J.T. Yates, Photocatalysis on TiO_2 surfaces – principles, mechanisms, and selected results, Chem. Rev. 95 (1995) 735–758.
[10] M.R. Hoffmann, S.T. Martin, W.Y. Choi, D.W. Bahnemann, Environmental applications of semiconductor photocatalysis, Chem. Rev. 95 (1995) 69–96.
[11] P.V. Kamat, Photochemistry on nonreactive and reactive (semiconductor) surfaces, Chem. Rev. 93 (1993) 267–300.
[12] M.A. Fox, M.T. Dulay, Heterogeneous photocatalysis, Chem. Rev. 93 (1993) 341–357.
[13] H.Q. Sun, S.B. Wang, Research advances in the synthesis of nanocarbon-based photocatalysts and their applications for photocatalytic conversion of carbon dioxide to hydrocarbon fuels, Energy Fuels 28 (2014) 22–36.
[14] H.Q. Sun, S.B. Wang, H.M. Ang, M.O. Tade, Q. Li, Halogen element modified titanium dioxide for visible light photocatalysis, Chem. Eng. J. 162 (2010) 437–447.
[15] Z.F. Huang, J.J. Song, L. Pan, X.W. Zhang, L. Wang, J.J. Zou, Tungsten oxides for photocatalysis, electrochemistry, and phototherapy, Adv. Mater. 27 (2015) 5309–5327.
[16] S.W. Cao, J.X. Low, J.G. Yu, M. Jaroniec, Polymeric photocatalysts based on graphitic carbon nitride, Adv. Mater. 27 (2015) 2150–2176.
[17] S.J.A. Moniz, S.A. Shevlin, D.J. Martin, Z.X. Guo, J.W. Tang, Visible-light driven heterojunction photocatalysts for water splitting – a critical review, Energy Environ. Sci. 8 (2015) 731–759.
[18] H.L. Wang, L.S. Zhang, Z.G. Chen, J.Q. Hu, S.J. Li, Z.H. Wang, J.S. Liu, X.C. Wang, Semiconductor heterojunction photocatalysts: design, construction, and photocatalytic performances, Chem. Soc. Rev. 43 (2014) 5234–5244.
[19] T. Hisatomi, J. Kubota, K. Domen, Recent advances in semiconductors for photocatalytic and photoelectrochemical water splitting, Chem. Soc. Rev. 43 (2014) 7520–7535.
[20] M.J. Kale, T. Avanesian, P. Christopher, Direct photocatalysis by plasmonic nanostructures, ACS Catal. 4 (2014) 116–128.
[21] S.N. Habisreutinger, L. Schmidt-Mende, J.K. Stolarczyk, Photocatalytic reduction of CO_2 on TiO_2 and other semiconductors, Angew. Chem. Int. Ed. 52 (2013) 7372–7408.
[22] W.B. Hou, S.B. Cronin, A review of surface plasmon resonance-enhanced photocatalysis, Adv. Funct. Mater. 23 (2013) 1612–1619.
[23] N. Liu, X.Y. Chen, J.L. Zhang, J.W. Schwank, A review on TiO_2-based nanotubes synthesized via hydrothermal method: formation mechanism, structure modification, and photocatalytic applications, Catal. Today 225 (2014) 34–51.
[24] S. Bai, J. Jiang, Q. Zhang, Y.J. Xiong, Steering charge kinetics in photocatalysis: intersection of materials syntheses, characterization techniques and theoretical simulations, Chem. Soc. Rev. 44 (2015) 2893–2939.
[25] J.D. Holladay, J. Hu, D.L. King, Y. Wang, An overview of hydrogen production technologies, Catal. Today 139 (2009) 244–260.
[26] R.M. Navarro, M.A. Pena, J.L.G. Fierro, Hydrogen production reactions from carbon feedstocks: fossils fuels and biomass, Chem. Rev. 107 (2007) 3952–3991.
[27] Y.H. Hu, E. Ruckenstein, Catalytic conversion of methane to synthesis gas by partial oxidation and CO_2 reforming, Adv. Catal. 48 (48) (2004) 297–345.
[28] R.W. Dorner, D.R. Hardy, F.W. Williams, H.D. Willauer, Heterogeneous catalytic CO_2 conversion to value-added hydrocarbons, Energy Environ. Sci. 3 (2010) 884–890.
[29] E.V. Kondratenko, G. Mul, J. Baltrusaitis, G.O. Larrazabal, J. Perez-Ramirez, Status and perspectives of CO_2 conversion into fuels and chemicals by catalytic, photocatalytic and electrocatalytic processes, Energy Environ. Sci. 6 (2013) 3112–3135.

[30] S.J.T. Pollard, G.D. Fowler, C.J. Sollars, R. Perry, Low-cost adsorbents for waste and waste-water treatment – a review, Sci. Total Environ. 116 (1992) 31–52.

[31] A. Bhatnagar, M. Sillanpaa, Utilization of agro-industrial and municipal waste materials as potential adsorbents for water treatment – a review, Chem. Eng. J. 157 (2010) 277–296.

[32] K.M. Smith, G.D. Fowler, S. Pullket, N.J.D. Graham, Sewage sludge-based adsorbents: a review of their production, properties and use in water treatment applications, Water Res. 43 (2009) 2569–2594.

[33] J. Benner, D.E. Helbling, H.P.E. Kohler, J. Wittebol, E. Kaiser, C. Prasse, T.A. Ternes, C.N. Albers, J. Aamand, B. Horemans, D. Springael, E. Walravens, N. Boon, Is biological treatment a viable alternative for micropollutant removal in drinking water treatment processes?, Water Res 47 (2013) 5955–5976.

[34] E. Neyens, J. Baeyens, A review of classic Fenton's peroxidation as an advanced oxidation technique, J. Hazard. Mater. 98 (2003) 33–50.

[35] J.J. Pignatello, E. Oliveros, A. MacKay, Advanced oxidation processes for organic contaminant destruction based on the Fenton reaction and related chemistry, Crit. Rev. Environ. Sci. Technol. 36 (2006) 1–84.

[36] M. Umar, H.A. Aziz, M.S. Yusoff, Trends in the use of Fenton, electro-Fenton and photo-Fenton for the treatment of landfill leachate, Waste Manage. 30 (2010) 2113–2121.

[37] B. Brunekreef, S.T. Holgate, Air pollution and health, Lancet 360 (2002) 1233–1242.

[38] S.B. Wang, H.M. Ang, M.O. Tade, Volatile organic compounds in indoor environment and photocatalytic oxidation: state of the art, Environ. Int. 33 (2007) 694–705.

[39] J. Gao, X. Peng, G. Chen, J. Xu, G.L. Shi, Y.C. Zhang, Y.C. Feng, Insights into the chemical characterization and sources of PM2.5 in Beijing at a 1-h time resolution, Sci. Total Environ. 542 (2016) 162–171.

[40] P. Brimblecombe, Z. Ning, Effect of road blockages on local air pollution during the Hong Kong protests and its implications for air quality management, Sci. Total Environ. 536 (2015) 443–448.

[41] Y. Zhuang, J.H. Pavlish, Fate of hazardous air pollutants in oxygen-fired coal combustion with different flue gas recycling, Environ. Sci. Technol. 46 (2012) 4657–4665.

[42] S.H. Byeon, B.K. Lee, B.R. Mohan, Removal of ammonia and particulate matter using a modified turbulent wet scrubbing system, Sep. Purif. Technol. 98 (2012) 221–229.

[43] C. Van der Heyden, P. Demeyer, E.I.P. Volcke, Mitigating emissions from pig and poultry housing facilities through air scrubbers and biofilters: state-of-the-art and perspectives, Biosyst. Eng. 134 (2015) 74–93.

[44] J.H. Mo, Y.P. Zhang, Q.J. Xu, J.J. Lamson, R.Y. Zhao, Photocatalytic purification of volatile organic compounds in indoor air: a literature review, Atmos. Environ. 43 (2009) 2229–2246.

[45] W.H. Organization, WHO Air Quality Guildlines Globle Update 2005, WHO Air Quality Guildlines, 2005.

[46] U. EPA, National Ambient Air Quality Standards (NAAQS), 1998.

[47] E.C. Environment, Air Quality Standards, European Union Policy on Air Quality, 2013.

[48] P.R.C. Environment, Ministry of Environmental Protection, GB 3095-2012 Ambient Air Quality Standard, Chinese National Ambient Air Quality Standards (CNAAQS), 2012.

[49] D.o.t. Environment, National Air Quality Standards, National Standards for Criteria Air Pollutants in Australia, 2005.

[50] J. Lasek, Y.H. Yu, J.C.S. Wu, Removal of NO$_x$ by photocatalytic processes, J. Photochem. Photobiol. C 14 (2013) 29–52.

[51] Y.X. Sun, E. Zwolinska, A.G. Chmielewski, Abatement technologies for high concentrations of NO$_x$ and SO$_2$ removal from exhaust gases: a review, Crit. Rev. Environ. Sci. Technol. 46 (2016) 119–142.

[52] J. Peral, X. Domenech, D.F. Ollis, Heterogeneous photocatalysis for purification, decontamination and deodorization of air, J. Chem. Technol. Biotechnol. 70 (1997) 117–140.

[53] J. Zhao, X.D. Yang, Photocatalytic oxidation for indoor air purification: a literature review, Build. Environ. 38 (2003) 645–654.

[54] S.W. Verbruggen, TiO$_2$ photocatalysis for the degradation of pollutants in gas phase: from morphological design to plasmonic enhancement, J. Photochem. Photobiol. C 24 (2015) 64–82.

[55] J.Z. Lyu, L.Z. Zhu, C. Burda, Considerations to improve adsorption and photocatalysis of low concentration air pollutants on TiO$_2$, Catal. Today 225 (2014) 24–33.

[56] L.X. Zhong, F. Haghighat, Photocatalytic air cleaners and materials technologies – abilities and limitations, Build. Environ. 91 (2015) 191–203.

[57] O. Legrini, E. Oliveros, A.M. Braun, Photochemical processes for water-treatment, Chem. Rev. 93 (1993) 671–698.

[58] J.H. Carey, J. Lawrence, H.M. Tosine, Photo-dechlorination of pcbs in presence of titanium-dioxide in aqueous suspensions, Bull. Environ. Contam. Toxicol. 16 (1976) 697–701.

[59] V.M. Daskalaki, M. Antoniadou, G.L. Puma, D.I. Kondarides, P. Lianos, Solar light-responsive Pt/CdS/TiO$_2$ photocatalysts for hydrogen production and simultaneous degradation of inorganic or organic sacrificial agents in wastewater, Environ. Sci. Technol. 44 (2010) 7200–7205.

[60] M. Formenti, F. Juillet, P. Meriaudeau, S.J. Teichner, Heterogeneous photocatalysis for partial oxidation of paraffins, Chem. Technol. 1 (1971) 680–681.

[61] R.I. Bickley, F.S. Stone, Photoadsorption and photocatalysis at rutile surfaces. 1. Photoadsorption of oxygen, J. Catal. 31 (1973) 389–397.

[62] T.X. Liu, F.B. Li, X.Z. Li, TiO$_2$ hydrosols with high activity for photocatalytic degradation of formaldehyde in a gaseous phase, J. Hazard. Mater. 152 (2008) 347–355.

[63] J. Peral, D.F. Ollis, Heterogeneous photocatalytic oxidation of gas-phase organics for air purification – acetone, 1-butanol, butyraldehyde, formaldehyde, and meta-xylene oxidation, J. Catal. 136 (1992) 554–565.

[64] T.N. Obee, R.T. Brown, TiO$_2$ photocatalysis for indoor air applications – effects of humidity and trace contaminant levels on the oxidation rates of formaldehyde, toluene, and 1,3-butadiene, Environ. Sci. Technol. 29 (1995) 1223–1231.

[65] J.J. Yang, D.X. Li, Z.J. Zhang, Q.L. Li, H.Q. Wang, A study of the photocatalytic oxidation of formaldehyde on Pt/Fe$_2$O$_3$/TiO$_2$, J. Photochem. Photobiol. A 137 (2000) 197–202.

[66] C.H. Ao, S.C. Lee, J.Z. Yu, J.H. Xu, Photodegradation of formaldehyde by photocatalyst TiO$_2$: effects on the presences of NO, SO$_2$ and VOCs, Appl. Catal. B 54 (2004) 41–50.

[67] F. Shiraishi, T. Nomura, S. Yamaguchi, Y. Ohbuchi, Rapid removal of trace HCHO from indoor air by an air purifier consisting of a continuous concentrator and photocatalytic reactor and its computer simulation, Chem. Eng. J. 127 (2007) 157–165.

[68] F. Shiraishi, D. Ohkubo, K. Toyoda, S. Yamaguchi, Decomposition of gaseous formaldehyde in a photocatalytic reactor with a parallel array of light sources – 1. Fundamental experiment for reactor design, Chem. Eng. J. 114 (2005) 153–159.

[69] H.M. Liu, Z.W. Lian, X.J. Ye, W.F. Shangguan, Kinetic analysis of photocatalytic oxidation of gas-phase formaldehyde over titanium dioxide, Chemosphere 60 (2005) 630–635.

[70] P. Chin, L.P. Yang, D.F. Ollis, Formaldehyde removal from air via a rotating adsorbent combined with a photocatalyst reactor: kinetic modeling, J. Catal. 237 (2006) 29–37.

[71] O. Debono, F. Thevenet, P. Gravejat, V. Hequet, C. Raillard, L. Lecoq, N. Locoge, Toluene photocatalytic oxidation at ppbv levels: kinetic investigation and carbon balance determination, Appl. Catal. B 106 (2011) 600–608.

[72] J. Jeong, K. Sekiguchi, K. Sakamoto, Photochemical and photocatalytic degradation of gaseous toluene using short-wavelength UV irradiation with TiO$_2$ catalyst: comparison of three UV sources, Chemosphere 57 (2004) 663–671.

[73] N. Quici, M.L. Vera, H. Choi, G.L. Puma, D.D. Dionysiou, M.I. Litter, H. Destaillats, Effect of key parameters on the photocatalytic oxidation of toluene at low concentrations in air under 254 + 185 nm UV irradiation, Appl. Catal. B 95 (2010) 312–319.

[74] V. Augugliaro, S. Coluccia, V. Loddo, L. Marchese, G. Martra, L. Palmisano, M. Schiavello, Photocatalytic oxidation of gaseous toluene on anatase TiO$_2$ catalyst: mechanistic aspects and FT-IR investigation, Appl. Catal. B 20 (1999) 15–27.

[75] M.C. Blount, J.L. Falconer, Characterization of adsorbed species on TiO$_2$ after photocatalytic oxidation of toluene, J. Catal. 200 (2001) 21–33.

[76] C. Belver, M.J. Lopez-Munoz, J.M. Coronado, J. Soria, Palladium enhanced resistance to deactivation of titanium dioxide during the photocatalytic oxidation of toluene vapors, Appl. Catal. B 46 (2003) 497–509.

[77] J.H. Huang, X.C. Wang, Y.D. Hou, X.F. Chen, L. Wu, X.Z. Fu, Degradation of benzene over a zinc germanate photocatalyst under ambient conditions, Environ. Sci. Technol. 42 (2008) 7387–7391.

[78] W. Wang, Y. Ku, Photocatalytic degradation of gaseous benzene in air streams by using an optical fiber photoreactor, J. Photochem. Photobiol. A 159 (2003) 47–59.

[79] V. Puddu, H. Choi, D.D. Dionysiou, G.L. Puma, TiO$_2$ photocatalyst for indoor air remediation: influence of crystallinity, crystal phase, and UV radiation intensity on trichloroethylene degradation, Appl. Catal. B 94 (2010) 211–218.

[80] M. Mohseni, Gas phase trichloroethylene (TCE) photooxidation and byproduct formation: photolysis vs. titania/silica based photocatalysis, Chemosphere 59 (2005) 335–342.

[81] H.H. Ou, S.L. Lo, Photocatalysis of gaseous trichloroethylene (TCE) over TiO$_2$: the effect of oxygen and relative humidity on the generation of dichloroacetyl chloride (DCAC) and phosgene, J. Hazard. Mater. 146 (2007) 302–308.

[82] J. Angelo, L. Andrade, L.M. Madeira, A. Mendes, An overview of photocatalysis phenomena applied to NO$_x$ abatement, J. Environ. Manage. 129 (2013) 522–539.

[83] E. Luevano-Hipolito, A. Martinez-de la Cruz, Q.L. Yu, H.J.H. Brouwers, Precipitation synthesis of WO$_3$ for NO$_x$ using PEG as template, Ceram. Int. 40 (2014) 12123–12128.

[84] E. Luevano-Hipolito, A. Martinez-de la Cruz, E. Lopez-Cuellar, Q.L. Yu, H.J.H. Brouwers, Synthesis, characterization and photocatalytic activity of WO$_3$/TiO$_2$ for NO removal under UV and visible light irradiation, Mater. Chem. Phys. 148 (2014) 208–213.

[85] E. Luevano-Hipolito, A. Martinez-de la Cruz, Q.L. Yu, H.J.H. Brouwers, Photocatalytic removal of nitric oxide by Bi$_2$Mo$_3$O$_{12}$ prepared by co-precipitation method, Appl. Catal. A 468 (2013) 322–326.

[86] N. Bowering, G.S. Walker, P.G. Harrison, Photocatalytic decomposition and reduction reactions of nitric oxide over Degussa P25, Appl. Catal. B 62 (2006) 208–216.

[87] N.W. Cant, J.R. Cole, Photocatalysis of the reaction between ammonia and nitric-oxide on TiO$_2$ surfaces, J. Catal. 134 (1992) 317–330.

[88] P. Krishnan, M.H. Zhang, Y.H. Cheng, D.T. Riang, L.E. Yu, Photocatalytic degradation of SO$_2$ using TiO$_2$-containing silicate as a building coating material, Constr. Build. Mater. 43 (2013) 197–202.

[89] Z. Topalian, G.A. Niklasson, C.G. Granqvist, L. Osterlund, Spectroscopic study of the photofixation of SO_2 on anatase TiO_2 thin films and their oleophobic properties, ACS Appl. Mater. Interfaces 4 (2012) 672–679.

[90] D.H. Xia, L.L. Hu, C. He, W.Q. Pan, T.S. Yang, Y.C. Yang, D. Shu, Simultaneous photocatalytic elimination of gaseous NO and SO_2 in a $BiOI/Al_2O_3$-padded trickling scrubber under visible light, Chem. Eng. J. 279 (2015) 929–938.

[91] O. Rosseler, C. Ulhaq-Bouillet, A. Bonnefont, S. Pronkin, E. Savinova, A. Louvet, V. Keller, N. Keller, Structural and electronic effects in bimetallic PdPt nanoparticles on TiO_2 for improved photocatalytic oxidation of CO in the presence of humidity, Appl. Catal. B 166 (2015) 381–392.

[92] A. Linsebigler, G.Q. Lu, J.T. Yates, CO photooxidation on TiO_2(1 1 0), J. Phys. Chem. 100 (1996) 6631–6636.

[93] A. Nishimura, T. Hisada, M. Hirota, M. Kubota, E. Hu, Using TiO_2 photocatalyst with adsorbent to oxidize carbon monoxide in rich hydrogen, Catal. Today 158 (2010) 296–304.

[94] Y.W. Lu, X.H. Zhao, M.Y. Wang, Z.L. Yang, X.J. Zhang, C.X. Yang, Feasibility analysis on photocatalytic removal of gaseous ozone in aircraft cabins, Build. Environ. 81 (2014) 42–50.

[95] B. Ohtani, S.W. Zhang, S. Nishimoto, T. Kagiya, Catalytic and photocatalytic decomposition of ozone at room-temperature over titanium(IV) oxide, J. Chem. Soc. Faraday Trans. 88 (1992) 1049–1053.

[96] H. Yao, A. Feilberg, Characterisation of photocatalytic degradation of odorous compounds associated with livestock facilities by means of PTR-MS, Chem. Eng. J. 277 (2015) 341–351.

[97] S.B. Riffat, X.L. Ma, Performance testing of an optimal photocatalytic mop fan air cleaning system, Int. J. Energy Res. 37 (2013) 1389–1396.

[98] A.P. Bhirud, S.D. Sathaye, R.P. Waichal, J.D. Ambekar, C.J. Park, B.B. Kale, In-situ preparation of $N-TiO_2$/graphene nanocomposite and its enhanced photocatalytic hydrogen production by H_2S splitting under solar light, Nanoscale 7 (2015) 5023–5034.

[99] Y.S. Shen, Y. Ku, Decomposition of gas-phase trichloroethene by the UV/TiO_2 process in the presence of ozone, Chemosphere 46 (2002) 101–107.

[100] F.I. Khan, A.Kr. Ghoshal, Removal of volatile organic compounds from polluted air, J. Loss Prev. Process Ind. 13 (2000) 527–545.

[101] L. Spanhel, H. Weller, A. Henglein, Photochemistry of semiconductor colloids. 22. Electron injection from illuminated cds into attached TiO_2 and ZnO particles, J. Am. Chem. Soc. 109 (1987) 6632–6635.

[102] A. Di Paola, E. Garcia-Lopez, G. Marci, L. Palmisano, A survey of photocatalytic materials for environmental remediation, J. Hazard. Mater. 211 (2012) 3–29.

[103] Y. Inoue, Photocatalytic water splitting by RuO_2-loaded metal oxides and nitrides with d(0)- and d(10)-related electronic configurations, Energy Environ. Sci. 2 (2009) 364–386.

[104] H.Q. Sun, G.L. Zhou, Y.X. Wang, A. Suvorova, S.B. Wang, A new metal-free carbon hybrid for enhanced photocatalysis, ACS Appl. Mater. Interfaces 6 (2014) 16745–16754.

[105] C.L. Bianchi, S. Gatto, C. Pirola, A. Naldoni, A. Di Michele, G. Cerrato, V. Crocella, V. Capucci, Photocatalytic degradation of acetone, acetaldehyde and toluene in gas-phase: comparison between nano and micro-sized TiO_2, Appl. Catal. B 146 (2014) 123–130.

[106] M. Le Bechec, N. Kinadjian, D. Ollis, R. Backov, S. Lacombe, Comparison of kinetics of acetone, heptane and toluene photocatalytic mineralization over TiO_2 microfibers and quartzel (R) mats, Appl. Catal. B 179 (2015) 78–87.

[107] F. He, J.L. Li, T. Li, G.X. Li, Solvothermal synthesis of mesoporous TiO_2: the effect of morphology, size and calcination progress on photocatalytic activity in the degradation of gaseous benzene, Chem. Eng. J. 237 (2014) 312–321.

[108] L. Ren, Y.Z. Li, J.T. Hou, J.L. Bai, M.Y. Mao, M. Zeng, X.J. Zhao, N. Li, The pivotal effect of the interaction between reactant and anatase TiO_2 nanosheets with exposed 001 facets on photocatalysis for the photocatalytic purification of VOCs, Appl. Catal. B 181 (2016) 625–634.

[109] Z. Liu, F.T. Chen, P.F. Fang, S.J. Wang, Y.P. Gao, F. Zheng, Y. Liu, Y.Q. Dai, Study of adsorption-assisted photocatalytic oxidation of benzene with TiO_2/SiO_2 nanocomposites, Appl. Catal. A 451 (2013) 120–126.

[110] H.B. Huang, H.L. Huang, L. Zhang, P. Hu, X.G. Ye, D.Y.C. Leung, Enhanced degradation of gaseous benzene under vacuum ultraviolet (VUV) irradiation over TiO_2 modified by transition metals, Chem. Eng. J. 259 (2015) 534–541.

[111] J.J. Murcia, M.C. Hidalgo, J.A. Navio, V. Vaiano, D. Sannino, P. Ciambelli, Cyclohexane photocatalytic oxidation on Pt/TiO_2 catalysts, Catal. Today 209 (2013) 164–169.

[112] Y.L. Chen, X.X. Cao, B.F. Gao, B.Z. Lin, A facile approach to synthesize N-doped and oxygen-deficient TiO_2 with high visible-light activity for benzene decomposition, Mater. Lett. 94 (2013) 154–157.

[113] T.D. Pham, B.K. Lee, Novel adsorption and photocatalytic oxidation for removal of gaseous toluene by V-doped TiO_2/PU under visible light, J. Hazard. Mater. 300 (2015) 493–503.

[114] F. Thevenet, C. Guillard, A. Rousseau, Acetylene photocatalytic oxidation using continuous flow reactor: gas phase and adsorbed phase investigation, assessment of the photocatalyst deactivation, Chem. Eng. J. 244 (2014) 50–58.

[115] R.A.R. Monteiro, S.M. Miranda, C. Rodrigues-Silva, J.L. Faria, A.M.T. Silva, R.A.R. Boaventura, V.J.P. Vilar, Gas phase oxidation of n-decane and PCE by photocatalysis using an annular photoreactor packed with a monolithic catalytic bed coated with P25 and PC500, Appl. Catal. B 165 (2015) 306–315.

[116] N.S. Andryushina, O.L. Stroyuk, Influence of colloidal graphene oxide on photocatalytic activity of nanocrystalline TiO_2 in gas-phase ethanol and benzene oxidation, Appl. Catal. B 148 (2014) 543–549.

[117] R. Tejasvi, M. Sharma, K. Upadhyay, Passive photo-catalytic destruction of air-borne VOCs in high traffic areas using TiO_2-coated flexible PVC sheet, Chem. Eng. J. 262 (2015) 875–881.

[118] W.-M. Hou, Y. Ku, Photocatalytic decomposition of gaseous isopropanol in a tubular optical fiber reactor under periodic UV-LED illumination, J. Mol. Catal. A: Chem. 374 (2013) 7–11.

[119] H. Xie, B.S. Liu, X.J. Zhao, Facile process to greatly improve the photocatalytic activity of the TiO_2 thin film on window glass for the photodegradation of acetone and benzene, Chem. Eng. J. 284 (2016) 1156–1164.

[120] A. Antonello, G. Soliveri, D. Meroni, G. Cappelletti, S. Ardizzone, Photocatalytic remediation of indoor pollution by transparent TiO_2 films, Catal. Today 230 (2014) 35–40.

[121] A. Banisharif, A.A. Khodadadi, Y. Mortazavi, A.A. Firooz, J. Beheshtian, S. Agah, S. Menbari, Highly active Fe_2O_3-doped TiO_2 photocatalyst for degradation of trichloroethylene in air under UV and visible light irradiation: experimental and computational studies, Appl. Catal. B 165 (2015) 209–221.

[122] D.X.M. Vargas, J.R. De la Rosa, C.J. Lucio-Ortiz, A. Hernandez-Ramirez, G.A. Flores-Escamilla, C.D. Garcia, Photocatalytic degradation of trichloroethylene in a continuous annular reactor using Cu-doped TiO_2 catalysts by sol-gel synthesis, Appl. Catal. B 179 (2015) 249–261.

[123] H.Q. Zhuang, Q. Gu, J.L. Long, H. Lin, H.X. Lin, X.X. Wang, Visible light-driven decomposition of gaseous benzene on robust Sn^{2+}-doped anatase TiO_2 nanoparticles, RSC Adv. 4 (2014) 34315–34324.

[124] Z.N. Han, V.W. Chang, X.P. Wang, T.T. Lim, L. Hildemann, Experimental study on visible-light induced photocatalytic oxidation of gaseous formaldehyde by polyester fiber supported photocatalysts, Chem. Eng. J. 218 (2013) 9–18.

[125] L. Szatmary, J. Subrt, V. Kalousek, J. Mosinger, K. Lang, Low-temperature deposition of anatase on nanofiber materials for photocatalytic NO_x removal, Catal. Today 230 (2014) 74–78.

[126] C.X. Wang, J.Z. Ma, F.D. Liu, H. He, R.D. Zhang, The effects of Mn^{2+} precursors on the structure and ozone decomposition activity of cryptomelane-type manganese oxide (OMS-2) catalysts, J. Phys. Chem. C 119 (2015) 23119–23126.

[127] J.Z. Ma, H. He, F.D. Liu, Effect of Fe on the photocatalytic removal of NO_x over visible light responsive Fe/TiO_2 catalysts, Appl. Catal. B 179 (2015) 21–28.

[128] Y. Hu, X. Song, S.M. Jiang, C.H. Wei, Enhanced photocatalytic activity of Pt-doped TiO_2 for NO_x oxidation both under UV and visible light irradiation: a synergistic effect of lattice Pt^{4+} and surface PtO, Chem. Eng. J. 274 (2015) 102–112.

[129] A. Alonso-Tellez, D. Robert, V. Keller, N. Keller, H_2S photocatalytic oxidation over WO_3/TiO_2 Hombikat UV100, Environ. Sci. Pollut. Res. 21 (2014) 3503–3514.

[130] Y.C. Jiao, H.L. Jiang, F. Chen, RuO_2/TiO_2/Pt ternary photocatalysts with epitaxial heterojunction and their application in CO oxidation, ACS Catal. 4 (2014) 2249–2257.

[131] N.H. Nguyen, H.Y. Wu, H.L. Bai, Photocatalytic reduction of NO_2 and CO_2 using molybdenum-doped titania nanotubes, Chem. Eng. J. 269 (2015) 60–66.

[132] W. Zhu, S.N. Xiao, D.Q. Zhang, P.J. Liu, H.J. Zhou, W.R. Dai, F.F. Liu, H.X. Li, Highly efficient and stable Au/CeO_2-TiO_2 photocatalyst for nitric oxide abatement: potential application in flue gas treatment, Langmuir 31 (2015) 10822–10830.

[133] A. Yamamoto, K. Teramura, S. Hosokawa, T. Shishido, T. Tanaka, Visible-light-assisted selective catalytic reduction of nitric oxide with ammonia over dye-modified titania photocatalysts, ChemCatChem 7 (2015) 1818–1825.

[134] N. Seifvand, E. Kowsari, Novel TiO_2/graphene oxide functionalized with a cobalt complex for significant degradation of NO_x and CO, RSC Adv. 5 (2015) 93706–93716.

[135] H. Liu, X.Q. Yu, H.M. Yang, The integrated photocatalytic removal of SO_2 and NO using Cu doped titanium dioxide supported by multi-walled carbon nanotubes, Chem. Eng. J. 243 (2014) 465–472.

[136] Y.C. Liao, C.S. Xie, Y. Liu, Q.W. Huang, Enhancement of photocatalytic property of ZnO for gaseous formaldehyde degradation by modifying morphology and crystal defect, J. Alloy. Compd. 550 (2013) 190–197.

[137] Y.C. Chen, K. Katsumata, Y.H. Chiu, K. Okada, N. Matsushita, Y.J. Hsu, ZnO-graphene composites as practical photocatalysts for gaseous acetaldehyde degradation and electrolytic water oxidation, Appl. Catal. A 490 (2015) 1–9.

[138] Q. Huang, W.J. Ma, X.K. Yan, Y.W. Chen, S.M. Zhu, S.B. Shen, Photocatalytic decomposition of gaseous HCHO by $Zr_xTi_{1-x}O_2$ catalysts under UV–vis light irradiation with an energy-saving lamp, J. Mol. Catal. A 366 (2013) 261–265.

[139] Z. Wan, G.K. Zhang, Synthesis and facet-dependent enhanced photocatalytic activity of Bi_2SiO_5/AgI nanoplate photocatalysts, J. Mater. Chem. A 3 (2015) 16737–16745.

[140] Y.J. Sun, T. Xiong, Z.L. Ni, J. Liu, F. Dong, W. Zhang, W.K. Ho, Improving $g-C_3N_4$ photocatalysis for NO_x removal by Ag nanoparticles decoration, Appl. Surf. Sci. 358 (2015) 356–362.

[141] K. Katsumata, R. Motoyoshi, N. Matsushita, K. Okada, Preparation of graphitic carbon nitride ($g-C_3N_4$)/WO_3 composites and enhanced visible-light-driven photodegradation of acetaldehyde gas, J. Hazard. Mater. 260 (2013) 475–482.

[142] R. Sugranez, J. Balbuena, M. Cruz-Yusta, F. Martin, J. Morales, L. Sanchez, Efficient behaviour of hematite towards the photocatalytic degradation of NO_x gases, Appl. Catal. B 165 (2015) 529–536.

[143] Y. Shen, L.F. Wang, Y.B. Wu, X.Y. Li, Q.D. Zhao, Y. Hou, W. Teng, Facile solvothermal synthesis of $MnFe_2O_4$ hollow nanospheres and their photocatalytic degradation of benzene investigated by in situ FTIR, Catal. Commun. 68 (2015) 11–14.

[144] Y.B. Chen, D.Z. Li, J. Chen, J.X. Wang, S.G. Meng, J.J. Xian, X.Z. Fu, Y. Shao, A promising new photocatalyst CdSnO₃ center dot 3H(2)O for air purification under ambient condition, Appl. Catal. B 129 (2013) 403–408.

[145] D.W. Huang, X.L. Fu, J.L. Long, X.L. Jiang, L. Chang, S.G. Meng, S.F. Chen, Hydrothermal synthesis of MSn(OH)(6) (M = Co, Cu, Fe, Mg, Mn, Zn) and their photocatalytic activity for the destruction of gaseous benzene, Chem. Eng. J. 269 (2015) 168–179.

[146] Z.R. Zhu, F.Y. Liu, W. Zhang, Fabricate and characterization of Ag/BaAl₂O₄ and its photocatalytic performance towards oxidation of gaseous toluene studied by FTIR spectroscopy, Mater. Res. Bull. 64 (2015) 68–75.

[147] M. Ou, Q. Zhong, S.L. Zhang, L.M. Yu, Ultrasound assisted synthesis of heterogeneous g-C₃N₄/BiVO₄ composites and their visible-light-induced photocatalytic oxidation of NO in gas phase, J. Alloy. Compd. 626 (2015) 401–409.

[148] A.Y. Shan, T.I.M. Ghazi, S.A. Rashid, Immobilisation of titanium dioxide onto supporting materials in heterogeneous photocatalysis: a review, Appl. Catal. A 389 (2010) 1–8.

[149] L. Lopez, W.A. Daoud, D. Dutta, B.C. Panther, T.W. Turney, Effect of substrate on surface morphology and photocatalysis of large-scale TiO₂ films, Appl. Surf. Sci. 265 (2013) 162–168.

[150] M.J. Sampaio, C.G. Silva, A.M.T. Silva, V.J.P. Vilar, R.A.R. Boaventura, J.L. Faria, Photocatalytic activity of TiO₂-coated glass raschig rings on the degradation of phenolic derivatives under simulated solar light irradiation, Chem. Eng. J. 224 (2013) 32–38.

[151] M. Kete, E. Pavlica, F. Fresno, G. Bratina, U.L. Stangar, Highly active photocatalytic coatings prepared by a low-temperature method, Environ. Sci. Pollut. Res. 21 (2014) 11238–11249.

[152] K. Tennakone, C.T.K. Tilakaratne, I.R.M. Kottegoda, Photocatalytic degradation of organic contaminants in water with TiO₂ supported on polythene films, J. Photochem. Photobiol. A 87 (1995) 177–179.

[153] J.C. Yu, J. Lin, D. Lo, S.K. Lam, Influence of thermal treatment on the adsorption of oxygen and photocatalytic activity of TiO(2), Langmuir 16 (2000) 7304–7308.

[154] D. Robert, V. Keller, N. Keller, Immobilization of a Semiconductor Photocatalyst on Solid Supports: Methods, Materials, and Applications, Photocatalysis and Water Purification, Wiley-VCH Verlag GmbH & Co. KGaA, 2013, pp. 145–178.

[155] C.W.H. Dunnill, Z.A. Aiken, J. Pratten, M. Wilson, D.J. Morgan, I.P. Parkin, Enhanced photocatalytic activity under visible light in N-doped TiO₂ thin films produced by APCVD preparations using t-butylamine as a nitrogen source and their potential for antibacterial films, J. Photochem. Photobiol. A 207 (2009) 244–253.

[156] M.G. Nolan, M.E. Pemble, D.W. Sheel, H.M. Yates, H.M. Yates, One step process for chemical vapour deposition of titanium dioxide thin films incorporating controlled structure nanoparticles, Thin Solid Films 515 (2006) 1956–1962.

[157] H. Nizard, M.L. Kosinova, N.I. Fainer, Y.M. Rumyantsev, B.M. Ayupov, Y.V. Shubin, Deposition of titanium dioxide from TTIP by plasma enhanced and remote plasma enhanced chemical vapor deposition, Surf. Coat. Technol. 202 (2008) 4076–4085.

[158] H.F. Sun, C.Y. Wang, S.H. Pang, X.P. Li, Y. Tao, H.J. Tang, M. Liu, Photocatalytic TiO₂ films prepared by chemical vapor deposition at atmosphere pressure, J. Non-Cryst. Solids 354 (2008) 1440–1443.

[159] D.N. Priya, J.M. Modak, A.M. Raichur, LbL fabricated poly(styrene sulfonate)/TiO₂ multilayer thin films for environmental applications, ACS Appl. Mater. Interfaces 1 (2009) 2684–2693.

[160] K.C. Krogman, N.S. Zacharia, D.M. Grillo, P.T. Hammond, Photocatalytic layer-by-layer coatings for degradation of acutely toxic agents, Chem. Mater. 20 (2008) 1924–1930.

[161] A. Nakajima, Y. Akiyama, S. Yanagida, T. Koike, T. Isobe, Y. Kameshima, K. Okada, Preparation and properties of Cu-grafted transparent TiO₂-nanosheet thin films, Mater. Lett. 63 (2009) 1699–1701.

[162] H.W. Chen, C.P. Liang, H.S. Huang, J.G. Chen, R. Vittal, C.Y. Lin, K.C.W. Wu, K.C. Ho, Electrophoretic deposition of mesoporous TiO₂ nanoparticles consisting of primary anatase nanocrystallites on a plastic substrate for flexible dye-sensitized solar cells, Chem. Commun. 47 (2011) 8346–8348.

[163] D.V. Bavykin, L. Passoni, F.C. Walsh, Hierarchical tube-in-tube structures prepared by electrophoretic deposition of nanostructured titanates into a TiO₂ nanotube array, Chem. Commun. 49 (2013) 7007–7009.

[164] N.S. Raddaha, L. Cordero-Arias, S. Cabanas-Polo, S. Virtanen, J.A. Roether, A.R. Boccaccini, Electrophoretic deposition of chitosan/h-BN and chitosan/h-BN/TiO₂ composite coatings on stainless steel (316L) substrates, Materials 7 (2014) 1814–1829.

[165] A. Chavez-Valdez, M. Herrmann, A.R. Boccaccini, Alternating current electrophoretic deposition (EPD) of TiO₂ nanoparticles in aqueous suspensions, J. Colloid Interface Sci. 375 (2012) 102–105.

[166] H.Q. Sun, G.L. Zhou, S.Z. Liu, H.M. Ang, M.O. Tade, S.B. Wang, Visible light responsive titania photocatalysts codoped by nitrogen and metal (Fe, Ni, Ag, or Pt) for remediation of aqueous pollutants, Chem. Eng. J. 231 (2013) 18–25.

[167] H.Q. Sun, Y. Bai, W.Q. Jin, N.P. Xu, Visible-light-driven TiO₂ catalysts doped with low-concentration nitrogen species, Sol. Energy Mater. Sol. Cells 92 (2008) 76–83.

[168] R. Ullah, H.Q. Sun, S.B. Wang, H.M. Ang, M.O. Tade, Wet-chemical synthesis of InTaO₄ for photocatalytic decomposition of organic contaminants in air and water with UV–vis light, Ind. Eng. Chem. Res. 51 (2012) 1563–1569.

[169] R. Ullah, H.Q. Sun, H.M. Ang, M.O. Tade, S.B. Wang, Visible light photocatalytic degradation of organics on nanoparticles of bi-metallic oxides, Sep. Purif. Technol. 89 (2012) 98–106.

[170] R. Ullah, H.Q. Sun, H.M. Ang, M.O. Tade, S.B. Wang, Photocatalytic oxidation of water and air contaminants with metal doped BiTaO₄ irradiated with visible light, Catal. Today 192 (2012) 203–212.

[171] H.Q. Sun, R. Ullah, S.H. Chong, H.M. Ang, M.O. Tade, S.B. Wang, Room-light-induced indoor air purification using an efficient Pt/N-TiO₂ photocatalyst, Appl. Catal. B 108 (2011) 127–133.

[172] Y. Boyjoo, M. Ang, V. Pareek, CFD simulation of a pilot scale slurry photocatalytic reactor and design of multiple-lamp reactors, Chem. Eng. Sci. 111 (2014) 266–277.

[173] Y. Boyjoo, M. Ang, V. Pareek, Lamp emission and quartz sleeve modelling in slurry photocatalytic reactors, Chem. Eng. Sci. 111 (2014) 34–40.

[174] S.W. Verbruggen, S. Lenaerts, S. Denys, Analytic versus CFD approach for kinetic modeling of gas phase photocatalysis, Chem. Eng. J. 262 (2015) 1–8.

[175] C. Passalía, O.M. Alfano, R.J. Brandi, A methodology for modeling photocatalytic reactors for indoor pollution control using previously estimated kinetic parameters, J. Hazard. Mater. 211–212 (2012) 357–365.

[176] G.E. Imoberdorf, A.E. Cassano, H.A. Irazoqui, O.M. Alfano, Optimal design and modeling of annular photocatalytic wall reactors, Catal. Today 129 (2007) 118–126.

[177] A.L.L. Zazueta, H. Destaillats, G. Li Puma, Radiation field modeling and optimization of a compact and modular multi-plate photocatalytic reactor (MPPR) for air/water purification by Monte Carlo method, Chem. Eng. J. 217 (2013) 475–485.

[178] A.O. Ibhadon, I.M. Arabatzis, P. Falaras, D. Tsoukleris, The design and photoreaction kinetic modeling of a gas-phase titania foam packed bed reactor, Chem. Eng. J. 133 (2007) 317–323.

[179] S. Adjimi, J.C. Roux, N. Sergent, F. Delpech, P.X. Thivel, M. Pera-Titus, Photocatalytic oxidation of ethanol using paper-based nano-TiO₂ immobilized on porous silica: a modelling study, Chem. Eng. J. 251 (2014) 381–391.

[180] V.H.A. van Dijk, G. Simmelink, G. Mul, The influence of water vapour on the photocatalytic oxidation of cyclohexane in an internally illuminated monolith reactor, Appl. Catal. A 470 (2014) 63–71.

[181] E. Taboada, I. Angurell, J. Llorca, Dynamic photocatalytic hydrogen production from ethanol-water mixtures in an optical fiber honeycomb reactor loaded with Au/TiO₂, J. Catal. 309 (2014) 460–467.

[182] W.M. Hou, Y. Ku, Photocatalytic decomposition of gaseous isopropanol in a tubular optical fiber reactor under periodic UV-LED illumination, J. Mol. Catal. A 374 (2013) 7–11.

[183] N. Doss, P. Bernhardt, T. Romero, R. Masson, V. Keller, N. Keller, Photocatalytic degradation of butanone (methylethylketone) in a small-size TiO₂/beta-SiC alveolar foam LED reactor, Appl. Catal. B 154 (2014) 301–308.

[184] M. Hajaghazadeh, V. Vaiano, D. Sannino, H. Kakooei, R. Sotudeh-Gharebagh, P. Ciambelli, Heterogeneous photocatalytic oxidation of methyl ethyl ketone under UV – a light in an LED-fluidized bed reactor, Catal. Today 230 (2014) 79–84.

[185] D.M. Lee, H.J. Yun, S. Yu, S.J. Yun, S.Y. Lee, S.H. Kang, J. Yi, Design of an efficient photocatalytic reactor for the decomposition of gaseous organic contaminants in air, Chem. Eng. J. 187 (2012) 203–209.

[186] H. Destaillats, M. Sleiman, D.P. Sullivan, C. Jacquiod, J. Sablayrolles, L. Molins, Key parameters influencing the performance of photocatalytic oxidation (PCO) air purification under realistic indoor conditions, Appl. Catal. B 128 (2012) 159–170.

[187] T.C. Wang, L.J. Yang, X.Z. Du, Y.P. Yang, Numerical investigation on CO₂ photocatalytic reduction in optical fiber monolith reactor, Energy Convers. Manage. 65 (2013) 299–307.

[188] M. Tahir, N.S. Amin, Photocatalytic CO₂ reduction with H₂O vapors using montmorillonite/TiO₂ supported microchannel monolith photoreactor, Chem. Eng. J. 230 (2013) 314–327.

[189] M. Singh, I. Salvadó-Estivill, G. Li Puma, Radiation field optimization in photocatalytic monolith reactors for air treatment, AIChE J. 53 (2007) 678–686.

[190] Q.L. Yu, H.J.H. Brouwers, Indoor air purification using heterogeneous photocatalytic oxidation. Part I: experimental study, Appl. Catal. B 92 (2009) 454–461.

[191] J.V. Staub de Melo, G. Triches, Evaluation of the influence of environmental conditions on the efficiency of photocatalytic coatings in the degradation of nitrogen oxides (NOₓ), Build. Environ. 49 (2012) 117–123.

[192] T. Guo, Z. Bai, C. Wu, T. Zhu, Influence of relative humidity on the photocatalytic oxidation (PCO) of toluene by TiO₂ loaded on activated carbon fibers: PCO rate and intermediates accumulation, Appl. Catal. B 79 (2008) 171–178.

[193] H. Einaga, S. Futamura, T. Ibusuki, Heterogeneous photocatalytic oxidation of benzene, toluene, cyclohexene and cyclohexane in humidified air: comparison of decomposition behavior on photoirradiated TiO₂ catalyst, Appl. Catal. B 38 (2002) 215–225.

[194] R.S. Zhu, S.A. Che, X.B. Liu, S.X. Lin, G.L. Xu, F. Ouyang, A novel fluidized-bed-optical-fibers photocatalytic reactor (FBOFPR) and its performance, Appl. Catal. A 471 (2014) 136–141.

[195] A.A. Assadi, J. Palau, A. Bouzaza, J. Penya-Roja, V. Martinez-Soriac, D. Wolbert, Abatement of 3-methylbutanal and trimethylamine with combined plasma and photocatalysis in a continuous planar reactor, J. Photochem. Photobiol. A 282 (2014) 1–8.

[196] A.A. Assadi, A. Bouzaza, C. Vallet, D. Wolbert, Use of DBD plasma, photocatalysis, and combined DBD plasma/photocatalysis in a continuous

annular reactor for isovaleraldehyde elimination – synergetic effect and byproducts identification, Chem. Eng. J. 254 (2014) 124–132.

[197] C. Passalía, O.M. Alfano, R.J. Brandi, Modeling and experimental verification of a corrugated plate photocatalytic reactor using computational fluid dynamics, Ind. Eng. Chem. Res. 50 (2011) 9077–9086.

[198] X. Wang, X. Tan, T. Yu, Modeling of formaldehyde photocatalytic degradation in a honeycomb monolith reactor using computational fluid dynamics, Ind. Eng. Chem. Res. 53 (2014) 18402–18410.

[199] S. Chong, S. Wang, M. Tadé, H.M. Ang, V. Pareek, Simulations of photodegradation of toluene and formaldehyde in a monolith reactor using computational fluid dynamics, AIChE J. 57 (2011) 724–734.

[200] S.R.-V. Castrillón, H. Ibrahim, H. De Lasa, Flow field investigation in a photocatalytic reactor for air treatment (photo-CREC–air), Chem. Eng. Sci. 61 (2006) 3343–3361.

[201] S. Romero-Vargas Castrillón, H.I. de Lasa, Performance evaluation of photocatalytic reactors for air purification using computational fluid dynamics (CFD), Ind. Eng. Chem. Res. 46 (2007) 5867–5880.

[202] C. Passalía, M.E. Martínez Retamar, O.M. Alfano, R.J. Brandi, Photocatalytic degradation of formaldehyde in gas phase on TiO$_2$ films: a kinetic study, Int. J. Chem. Reactor Eng. 8 (2010).

[203] A. Queffeulou, L. Geron, C. Archambeau, H.L. Gall, P.-M. Marquaire, O. Zahraa, Kinetic study of acetaldehyde photocatalytic oxidation with a thin film of TiO$_2$ coated on stainless steel and CFD modeling approach, Ind. Eng. Chem. Res. 49 (2010) 6890–6897.

[204] X. Wang, X. Tan, T. Yu, Kinetic study of ozone photocatalytic decomposition using a thin film of TiO$_2$ coated on a glass plate and the CFD modeling approach, Ind. Eng. Chem. Res. 53 (2014) 7902–7909.

[205] K. Demeestere, A. De Visscher, J. Dewulf, M. Van Leeuwen, H. Van Langenhove, A new kinetic model for titanium dioxide mediated heterogeneous photocatalytic degradation of trichloroethylene in gas-phase, Appl. Catal. B 54 (2004) 261–274.

[206] B. Boulinguiez, A. Bouzaza, S. Merabet, D. Wolbert, Photocatalytic degradation of ammonia and butyric acid in plug-flow reactor: degradation kinetic modeling with contribution of mass transfer, J. Photochem. Photobiol. A 200 (2008) 254–261.

[207] V. Tomašić, F. Jović, Z. Gomzi, Photocatalytic oxidation of toluene in the gas phase: modelling an annular photocatalytic reactor, Catal. Today 137 (2008) 350–356.

[208] G.E. Imoberdorf, H.A. Irazoqui, O.M. Alfano, A.E. Cassano, Scaling-up from first principles of a photocatalytic reactor for air pollution remediation, Chem. Eng. Sci. 62 (2007) 793–804.

[209] F.V. Lopes, R.A. Monteiro, A.M. Silva, G.V. Silva, J.L. Faria, A.M. Mendes, V.J. Vilar, R.A. Boaventura, Insights into UV-TiO$_2$ photocatalytic degradation of PCE for air decontamination systems, Chem. Eng. J. 204 (2012) 244–257.

[210] V. Pareek, S. Chong, M. Tadé, A.A. Adesina, Light intensity distribution in heterogenous photocatalytic reactors, Asia-Pac. J. Chem. Eng. 3 (2008) 171–201.

[211] A.E. Cassano, C.A. Martin, R.J. Brandi, O.M. Alfano, Photoreactor analysis and design: fundamentals and applications, Ind. Eng. Chem. Res. 34 (1995) 2155–2201.

[212] Y. Boyjoo, M. Ang, V. Pareek, Some aspects of photocatalytic reactor modeling using computational fluid dynamics, Chem. Eng. Sci. 101 (2013) 764–784.

[213] R. Sharmin, M.B. Ray, Application of ultraviolet light-emitting diode photocatalysis to remove volatile organic compounds from indoor air, J. Air Waste Manag. Assoc. 62 (2012) 1032–1039.

[214] Z. Wang, J. Liu, Y. Dai, W. Dong, S. Zhang, J. Chen, CFD modeling of a UV-LED photocatalytic odor abatement process in a continuous reactor, J. Hazard. Mater. 215 (2012) 25–31.

[215] T.S. Natarajan, K. Natarajan, H.C. Bajaj, R.J. Tayade, Energy efficient UV-LED source and TiO$_2$ nanotube array-based reactor for photocatalytic application, Ind. Eng. Chem. Res. 50 (2011) 7753–7762.

[216] M.J. Muñoz-Batista, M. de los Milagros Ballari, A. Kubacka, A.E. Cassano, O.M. Alfano, M. Fernández-García, Acetaldehyde degradation under UV and visible irradiation using CeO$_2$–TiO$_2$ composite systems: evaluation of the photocatalytic efficiencies, Chem. Eng. J. 255 (2014) 297–306.

[217] G.E. Imoberdorf, A.E. Cassano, O.M. Alfano, H.A. Irazoqui, Modeling of a multiannular photocatalytic reactor for perchloroethylene degradation in air, AIChE J. 52 (2006) 1814–1823.

[218] M.J. Muñoz-Batista, A. Kubacka, M.N. Gómez-Cerezo, D. Tudela, M. Fernández-García, Sunlight-driven toluene photo-elimination using CeO$_2$-TiO$_2$ composite systems: a kinetic study, Appl. Catal. B 140 (2013) 626–635.

[219] L. Zhang, W.A. Anderson, A finite model for the prediction of the UV radiation field around a linear lamp, Chem. Eng. Sci. 65 (2010) 1513–1521.

[220] I. Salvadó-Estivill, D.M. Hargreaves, G. Li Puma, Evaluation of the intrinsic photocatalytic oxidation kinetics of indoor air pollutants, Environ. Sci. Technol. 41 (2007) 2028–2035.

[221] S. Elyasi, F. Taghipour, Simulation of UV photoreactor for degradation of chemical contaminants: model development and evaluation, Environ. Sci. Technol. 44 (2010) 2056–2063.

[222] J.E. Duran, F. Taghipour, M. Mohseni, Irradiance modeling in annular photoreactors using the finite-volume method, J. Photochem. Photobiol. A 215 (2010) 81–89.

[223] G.E. Imoberdorf, F. Taghipour, M. Mohseni, Radiation field modeling of multi-lamp, homogeneous photoreactors, J. Photochem. Photobiol. A 198 (2008) 169–178.

[224] V. Palma, D. Sannino, V. Vaiano, P. Ciambelli, Fluidized-bed reactor for the intensification of gas-phase photocatalytic oxidative dehydrogenation of cyclohexane, Ind. Eng. Chem. Res. 49 (2010) 10279–10286.

[225] R. Yang, Y.-P. Zhang, R.-Y. Zhao, An improved model for analyzing the performance of photocatalytic oxidation reactors in removing volatile organic compounds and its application, J. Air Waste Manag. Assoc. 54 (2004) 1516–1524.

[226] A.A. Assadi, A. Bouzaza, D. Wolbert, Photocatalytic oxidation of trimethylamine and isovaleraldehyde in an annular reactor: influence of the mass transfer and the relative humidity, J. Photochem. Photobiol. A 236 (2012) 61–69.

[227] R.A. Monteiro, F.V. Lopes, A.M. Silva, J. Ângelo, G.V. Silva, A.M. Mendes, R.A. Boaventura, V.J. Vilar, Are TiO$_2$-based exterior paints useful catalysts for gas-phase photooxidation processes? A case study on n-decane abatement for air detoxification, Appl. Catal. B 147 (2014) 988–999.

[228] I. Arabatzis, N. Spyrellis, Z. Loizos, P. Falaras, Design and theoretical study of a packed bed photoreactor, J. Mater. Process. Technol. 161 (2005) 224–228.

[229] G.L. Puma, I. Salvadó-Estivill, T.N. Obee, S.O. Hay, Kinetics rate model of the photocatalytic oxidation of trichloroethylene in air over TiO$_2$ thin films, Sep. Purif. Technol. 67 (2009) 226–232.

[230] F.V. Lopes, S.M. Miranda, R.A. Monteiro, S.D. Martins, A.M. Silva, J.L. Faria, R.A. Boaventura, V.J. Vilar, Perchloroethylene gas-phase degradation over titania-coated transparent monoliths, Appl. Catal. B 140 (2013) 444–456.

[231] T.N. Obee, Photooxidation of sub-parts-per-million toluene and formaldehyde levels on titania using a glass-plate reactor, Environ. Sci. Technol. 30 (1996) 3578–3584.

[232] C. Passalía, O.M. Alfano, R.J. Brandi, Optimal design of a corrugated-wall photocatalytic reactor using efficiencies in series and computational fluid dynamics (CFD) modeling, Ind. Eng. Chem. Res. 52 (2013) 6916–6922.

[233] G.E. Imoberdorf, H.A. Irazoqui, A.E. Cassano, O.M. Alfano, Photocatalytic degradation of tetrachloroethylene in gas phase on TiO$_2$ films: a kinetic study, Ind. Eng. Chem. Res. 44 (2005) 6075–6085.

[234] Q. Geng, Q. Guo, X. Yue, Adsorption and photocatalytic degradation kinetics of gaseous cyclohexane in an annular fluidized bed photocatalytic reactor, Ind. Eng. Chem. Res. 49 (2010) 4644–4652.

[235] H. Kisch, D. Bahnemann, Best practice in photocatalysis: comparing rates or apparent quantum yields?, J Phys. Chem. Lett. 6 (2015) 1907–1910.

[236] J. Peral, D.F. Ollis, Heterogeneous photocatalytic oxidation of gas-phase organics for air purification: acetone, 1-butanol, butyraldehyde, formaldehyde, and m-xylene oxidation, J. Catal. 136 (1992) 554–565.

[237] B. Serrano, H. De Lasa, Photocatalytic degradation of water organic pollutants. Kinetic modeling and energy efficiency, Ind. Eng. Chem. Res. 36 (1997) 4705–4711.

[238] G.E. Imoberdorf, A.E. Cassano, H.A. Irazoqui, O.M. Alfano, Simulation of a multi-annular photocatalytic reactor for degradation of perchloroethylene in air: parametric analysis of radiative energy efficiencies, Chem. Eng. Sci. 62 (2007) 1138–1154.

[239] C. Esterkin, A. Negro, O. Alfano, A. Cassano, Air pollution remediation in a fixed bed photocatalytic reactor coated with TiO$_2$, AIChE J. 51 (2005) 2298–2310.

[240] G.E. Imoberdorf, O.M. Alfano, A.E. Cassano, H.A. Irazoqui, Monte Carlo model of UV-radiation interaction with TiO$_2$-coated spheres, AIChE J. 53 (2007) 2688–2703.

[241] G. Imoberdorf, G. Vella, A. Sclafani, L. Rizzuti, O. Alfano, A. Cassano, Radiation model of a TiO$_2$-coated, quartz wool, packed-bed photocatalytic reactor, AIChE J. 56 (2010) 1030–1044.

[242] A. Alexiadis, 2-D radiation field in photocatalytic channels of square, rectangular, equilateral triangular and isosceles triangular sections, Chem. Eng. Sci. 61 (2006) 516–525.

[243] M.M. Hossain, G.B. Raupp, Polychromatic radiation field model for a honeycomb monolith photocatalytic reactor, Chem. Eng. Sci. 54 (1999) 3027–3034.

[244] M.M. Hossain, G.B. Raupp, Radiation field modeling in a photocatalytic monolith reactor, Chem. Eng. Sci. 53 (1998) 3771–3780.

[245] A.A. Assadi, A. Bouzaza, S. Merabet, D. Wolbert, Modeling and simulation of VOCs removal by nonthermal plasma discharge with photocatalysis in a continuous reactor: synergetic effect and mass transfer, Chem. Eng. J. 258 (2014) 119–127.

[246] A.A. Assadi, J. Palau, A. Bouzaza, D. Wolbert, Modeling of a continuous photocatalytic reactor for isovaleraldehyde oxidation: effect of different operating parameters and chemical degradation pathway, Chem. Eng. Res. Des. 91 (2013) 1307–1316.

[247] A. Motamed Dashliborun, R. Sotudeh-Gharebagh, M. Hajaghazadeh, H. Kakooei, S. Afshar, Modeling of the photocatalytic degradation of methyl ethyl ketone in a fluidized bed reactor of nano-TiO$_2$/γ-Al$_2$O$_3$ particles, Chem. Eng. J. 226 (2013) 59–67.

[248] M. Hossain, G.B. Raupp, S.O. Hay, T.N. Obee, Three-dimensional developing flow model for photocatalytic monolith reactors, AIChE J. 45 (1999) 1309–1321.

[249] H. Einaga, J. Tokura, Y. Teraoka, K. Ito, Kinetic analysis of TiO$_2$-catalyzed heterogeneous photocatalytic oxidation of ethylene using computational fluid dynamics, Chem. Eng. J. 263 (2015) 325–335.

[250] M. Mohseni, F. Taghipour, Experimental and CFD analysis of photocatalytic gas phase vinyl chloride (VC) oxidation, Chem. Eng. Sci. 59 (2004) 1601–1609.

[251] F. Jović, V. Kosar, V. Tomašić, Z. Gomzi, Non-ideal flow in an annular photocatalytic reactor, Chem. Eng. Res. Des. 90 (2012) 1297–1306.

[252] I. Salvadó-Estivill, A. Brucato, G. Li Puma, Two-dimensional modeling of a flat-plate photocatalytic reactor for oxidation of indoor air pollutants, Ind. Eng. Chem. Res. 46 (2007) 7489–7496.

[253] A. Queffeulou, L. Geron, E. Schaer, Prediction of photocatalytic air purifier apparatus performances with a CFD approach using experimentally determined kinetic parameters, Chem. Eng. Sci. 65 (2010) 5067–5074.

[254] <http://www.iphotocat.com/>.

[255] A. Mills, C. Hill, P.K.J. Robertson, Overview of the current ISO tests for photocatalytic materials, J. Photochem. Photobiol. A 237 (2012) 7–23.